fluids

MDPI

Review

Fluid Application Technologies in Plant Protection and Irrigation: A Review from Droplet Dynamics to Sprayers and Sprinklers

Si-Liang Sun [1], Jian-Hui Gui [2], Kai Dong [3,*] and Wei Zhang [1,*]

[1] School of Energy and Power Engineering, Jiangsu University, Zhenjiang 212013, China; sunsiliang@ujs.edu.cn
[2] Shimge (Zhejiang) Co., Ltd., Taizhou 317509, China; guijianhui@shimge.com
[3] Hangzhou International Innovation Institute, Beihang University, Hangzhou 311115, China
* Correspondence: radioaction@163.com (K.D.); zhangwei0112@ujs.edu.cn (W.Z.)

Abstract

Plant protection and sprinkler irrigation rely on common fluid dynamic processes, including liquid atomization, droplet transport, target interaction, and flow distribution. This review analyses these mechanisms within a multi-scale framework. The analysis starts with droplet–target interactions. It addresses droplet impact and foliar retention in plant protection, alongside droplet kinetic energy and soil-surface responses in irrigation. The discussion then extends to the spatial transport and distribution of sprays. At the device scale, this work examines nozzles and sprinklers from the perspective of fluid mechanics and structural innovation, detailing how nozzle geometry and flow conditions affect macroscopic application performance. Finally, this review addresses advances at the system scale, with a focus on energy consumption and data-driven performance prediction. By connecting fluid behavior across multiple spatial scales, this work links micro-scale droplet dynamics to whole-system performance and identifies directions for improving agricultural spraying and sprinkler irrigation systems.

Keywords: droplet; nozzle; sprayer; sprinkler; spray drift; spatial distribution uniformity

1. Introduction

Agriculture faces increasing pressure to improve resource-use efficiency while maintaining crop productivity [1,2]. Two important agricultural practices are agrochemical application for plant protection and water application through irrigation [3,4]. These functions are primarily performed by plant-protection sprayers and irrigation sprinklers. In irrigation, sprinkler systems are designed to distribute water uniformly while reducing runoff and evaporation losses [5,6]. For plant protection, nozzles affect droplet size spectra and spray transport to improve canopy coverage and reduce off-target losses [7].

Although plant protection and irrigation serve different agricultural purposes, both rely on the breakup of a continuous liquid into droplets with a range of sizes and velocities. Droplet size and velocity influence transport, deposition, target interaction, and environmental losses. In pesticide application, droplet characteristics require careful regulation to suppress wind-induced drift and off-target deposition. In irrigation, droplet momentum and impact energy need appropriate tuning to alleviate soil crusting, surface runoff and erosion. In both cases, system performance depends on droplet formation, transport, and interactions with the target surfaces.

Historically, research in these two fields developed largely independently. Studies on plant protection concentrate on atomization, drift reduction, canopy deposition and

Check for updates

Academic Editor: Markus Klein

Received: 20 June 2026
Revised: 4 August 2026
Accepted: 5 August 2026
Published: 11 August 2026

Copyright: © 2026 by the authors. Licensee MDPI, Basel, Switzerland. This article is an open access article distributed under the terms and conditions of the Creative Commons Attribution (CC BY) license.

foliar retention, whereas irrigation research emphasizes water distribution uniformity, soil infiltration, and runoff management [8]. Advances in precision agriculture, variable-rate application, and autonomous spraying systems have made the overlaps between the two fields more evident. However, existing reviews examine pesticide spraying or sprinkler irrigation separately, and few directly compare their equipment design and underlying fluid dynamics. Because both systems share governing principles for atomization and droplet transport, such a comparison may identify mechanisms and design considerations that are transferable between the two fields. This review adopts a multi-scale framework covering droplet generation, spray transport, hydraulic design, and energy optimization to compare plant-protection spraying and sprinkler irrigation.

The remainder of this paper is organized as follows. Section 2 examines droplet formation and target interaction. Section 3 discusses spray transport processes, including drift control and distribution uniformity. Section 4 reviews hydraulic advances in nozzles and sprinklers. Section 5 discusses energy efficiency and intelligent optimization, and Section 6 concludes the review with future perspectives. Figure 1 presents a coupling framework of agricultural spraying that explicitly links processes across different scales.

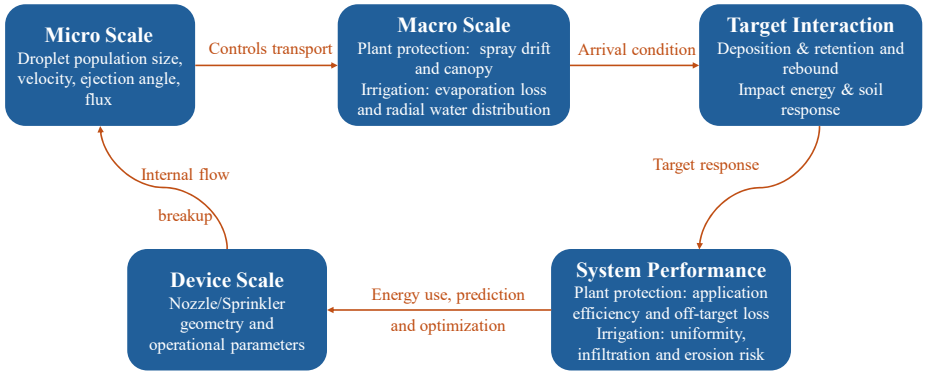


Figure 1. Multi-scale framework of agricultural liquid spraying systems.

2. Micro-Scale: Physical Characteristics and Target Interaction of Droplets

In agricultural fluid applications, droplets are the basic units governing atomization, transport, and target interaction. After discharge from the nozzle, droplet behavior is controlled by a combination of physical and interfacial properties, including droplet diameter (or volumetric median diameter, VMD), impact velocity and angle, surface tension, viscosity, density, charge, evaporation characteristics, and target-surface wettability [9–11]. These factors influence transport losses and deposition outcomes on the target surface.

In plant protection, these factors influence canopy penetration and subsequent behavior on leaf surfaces, including adhesion, spreading, rebound, splashing, deposition, and runoff [12]. Initial capture contributes to foliar interception, whereas the fraction remaining after rebound, splash, and runoff determines leaf retention. As shown in Figure 2, droplet–foliage interactions are influenced by three main groups of factors: droplet physicochemical properties, droplet impact parameters, and foliage surface and motion characteristics [13].

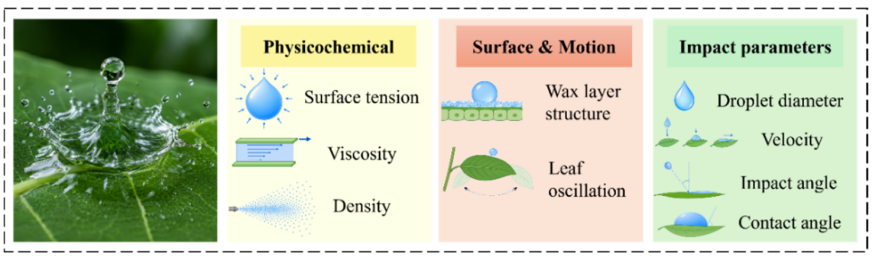


Figure 2. Factors affecting the target–droplet impact process.

In sprinkler irrigation, droplet-scale variables are primarily reflected in the energy delivered to the soil surface. Droplet diameter and impact velocity determine single-droplet kinetic energy and kinetic energy per unit droplet volume (KEd), whereas droplet flux, application rate (AR), and irrigation duration determine specific power (SP) and cumulative droplet kinetic energy per unit area (KEa) [6,14]. These energy-related parameters provide a more direct description of soil-surface loading than droplet size alone and are closely associated with infiltration reduction, runoff initiation, surface sealing or crusting, and soil erosion.

2.1. Plant-Protection Focus: Droplet Impact and Foliar Retention

After impacting foliage, spray droplets may spread and recoil. Depending on droplet inertia, formulation, and leaf surface properties, they may adhere, rebound, shatter, splash, or run off. Initial capture determines foliar interception, whereas the fraction remaining after rebound, splash, and runoff determines leaf retention [9,15]. Therefore, effective pesticide spraying requires both canopy penetration and post-impact capture on leaf surfaces.

Studies on ideal solid surfaces provide the physical basis for interpreting droplet impact on leaves. Using high-speed imaging, Šikalo and Ganić [16] identified deposition, rebound, and splash as typical outcomes of droplet–surface interaction and related these outcomes to droplet properties and surface conditions. The Weber number ($We = \rho v^2 D/\gamma$) describes the ratio of impact inertia to surface tension [17]. A higher Weber number indicates stronger inertial forcing and generally promotes spreading; whether a droplet undergoes adhesion, rebound, shattering, or splashing still depends on leaf wettability, roughness, and formulation properties.

Recent studies have extended droplet impact research from smooth plates and inclined surfaces to real crop leaves. On hydrophobic foliage such as rice leaves, droplets typically spread and recoil before entering adhesion, rebound, or shatter regimes. The boundaries between these regimes overlap in size–velocity space rather than being sharply separated. Smaller and slower droplets are more likely to adhere, whereas larger or faster droplets carry higher impact energy and are more prone to rebound or shatter [15]. On flexible leaves such as pepper leaves, part of the droplet impact energy is absorbed through leaf bending and torsion, which alters the spreading and recoil process [18]. On vibrating wheat leaves, leaf motion can further modify near-critical impact behavior, increase the spreading area, and modify the probability of deposition or sliding [19]. These results indicate that real leaves should not be treated as rigid, smooth, or stationary targets.

At the leaf scale, spray performance should be evaluated in terms of the amount intercepted, its spatial distribution, and the fraction retained after impact. Maximum retention (R_{max}) represents the highest liquid load reached before substantial runoff begins, whereas stable retention (R_{st}) represents the amount remaining after runoff and redistribution have largely ceased. In vivo measurements show that retention dynamics are species dependent and evolve through distinct temporal stages; accordingly, R_{max} and R_{st} should not be used interchangeably [13]. Coverage rate and its coefficient of variation are useful engineering indicators to describe deposition amount and uniformity, although collector-based measurements do not directly represent stable retention on real leaves [20]. Using high-speed imaging of cooling sprays, Aksoy et al. [21] derived Weber-number-based correlations for droplet spreading and recoil. These correlations provide a useful comparison, but their applicability to flexible leaf surfaces requires further validation.

Plant-protection research focuses on retaining liquid on flexible biological surfaces and commonly uses the Weber number and retention metrics, whereas irrigation research focuses on the kinetic-energy load delivered to the soil surface. Reported critical Weber numbers separating adhesion, rebound, and splash vary among studies because of dif-

ferences in leaf roughness, flexibility, liquid formulation, and measurement conditions. Moreover, most laboratory studies examine isolated leaves under static conditions and do not represent repeated droplet impacts, leaf vibration, and droplet interactions in crop canopies.

2.2. Irrigation Focus: Droplet Kinetic Energy and Soil-Surface Response

In sprinkler irrigation, droplets are evaluated by water delivery and impact energy. A key requirement is uniform application with limited disturbance to the soil surface. Fine droplets have lower individual impact energy [22] but are more vulnerable to wind drift and evaporation losses, whereas coarse droplets are more stable during transport but can generate higher momentum and kinetic energy upon impact [5,11]. Irrigation design involves a tradeoff between transport losses and soil-impact risk. The droplet population should be characterized by the distributions of droplet diameter, velocity at landing, flux, and impact energy, rather than a single representative diameter.

Recent studies have shifted from diameter-based descriptions toward energy-based characterization of soil impact. Chen et al. [6] conducted soil-container experiments using Nelson R33LP and R33 sprinklers and droplet-energy indicators (KEd, SP, and KEa) related to runoff, infiltration, crusting, and erosion processes. They showed that soil response depends on both AR and kinetic-energy loading. AR and SP were associated with runoff initiation and evolution, while SP and KEa were more closely related to final infiltration rate, surface sealing, and erosion development. Jiang et al. [14] used a two-dimensional video disdrometer to measure droplet size, velocity, and energy distributions, showing that droplet energy varies with nozzle geometry, operating pressure, and radial distance from the sprinkler. These results indicate that sprinkler droplets are better represented by coupled size–velocity–flux–energy distributions rather than by VMD or mean diameter alone.

Droplet-energy analysis clarifies the role of operating pressure. Lower pressure can reduce pumping energy but does not necessarily reduce soil-impact risk. When jet breakup is insufficient, low-pressure operation may produce larger droplets and localized peaks in AR and SP. In a study of low-pressure rotating sprinklers, Chen et al. [23] reported larger droplets and local peaks in AR and SP at the lowest tested pressure and did not recommend operation below 150 kPa under those conditions. Wang et al. [24] found that low pressure, especially with large nozzles, produced large droplets with high single-droplet kinetic energy and poorer spatial uniformity of SP, leading the authors to advise against operation below 250 kPa. Operating pressure affects the droplet spectrum and energy distribution and cannot alone indicate soil-impact risk.

Sprinkler structure can regulate droplet energy before impact. Nozzle geometry [25], orifice aspect ratio, diffuser design, and aeration alter droplet size, landing velocity, flux distribution, and kinetic-energy intensity [24,26]. Studies on circular and non-circular nozzles show that improved hydraulic uniformity does not necessarily guarantee lower soil-impact risk, because some configurations can still produce uneven kinetic-energy distribution or local SP peaks [10,24,26]. Structural changes should be evaluated by how they redistribute the droplet spectrum and impact energy, not only by hydraulic uniformity.

The agronomic effects of droplet-energy input arise through soil-surface processes and root-zone water dynamics. Moderate and spatially uniform water and energy inputs support infiltration and soil-water replenishment, whereas excessive local AR, SP, or KEa can detach soil particles, seal surface pores, increase crust bulk density, reduce infiltration capacity, and enhance runoff and soil loss [6]. Crop response to droplet energy is mediated by soil hydraulic behavior. Crop canopies may attenuate part of the incoming droplet energy before it reaches the soil.

Plant-protection spraying and sprinkler irrigation share basic fluid-dynamic principles but have different droplet-level objectives. Plant protection balances the inertia required for canopy penetration against rebound, splash, and runoff losses. Irrigation balances transport stability against soil-impact energy. Research in the two fields has developed separately, and empirical models are difficult to transfer because target properties and performance criteria differ. Work toward a unified droplet-prediction framework for both fields remains limited.

3. Macro-Scale: Spatial Spray Transport, Penetration, and Distribution

The macro-scale examines the collective transport and spatial distribution of droplets, complementing the micro-scale analysis of droplet–target interactions.

3.1. Plant-Protection Transport: Spray Drift Mitigation and Deposition Enhancement

3.1.1. Spray Losses and Dynamic Response Strategies

Spray atomization and flow fields are characterized using complementary experimental and computational methods. Laser diffraction measures volume-based droplet-size distributions; phase Doppler anemometry (PDA) provides pointwise measurements of individual droplet size and velocity; particle image velocimetry (PIV) resolves planar velocity fields of a selected phase; and patternators quantify the spatial distribution of collected spray liquid. CFD is widely used to simulate nozzle flow, liquid breakup, and droplet transport, whereas machine-learning models provide rapid, data-driven estimates of spray characteristics. Each approach has limitations. Laser diffraction measurements may be biased by non-uniform droplet velocities or incompletely atomized liquid ligaments. PDA and PIV require adequate optical access and become less reliable in dense sprays. Patternators quantify bulk liquid distribution but cannot capture droplet size or velocity information. CFD predictions depend on the selected turbulence and multi-phase models, mesh resolution, and boundary conditions, while machine-learning predictions are constrained by the range and quality of the training data. Experimental uncertainty affects both CFD validation and data-driven prediction.

During transport from the nozzle to the target, spray losses arise mainly from drift and evaporation. Droplet size is a major factor affecting both processes. Fine droplets have low inertia and short relaxation times [27], making them sensitive to crosswind and turbulent fluctuations; their large surface-area-to-volume ratio also accelerates evaporation under hot and dry conditions [28]. Larger droplets are less prone to drift but may reduce coverage uniformity and increase rebound or runoff upon impact.

Droplet motion in a crosswind is governed by the balance between aerodynamic drag, gravity, and buoyancy [29]:

$$\frac{dV_i}{dt} = \frac{3}{4}\frac{\rho C_D}{\rho_l \varnothing}(U_i - V_i)|U_i - V_i| - g_i\delta_{i3} \quad (1)$$

where V_i represents the velocity of the liquid particle, U_i is the air velocity and C_D is the dynamic drag coefficient depends on the particle diameter $\varnothing$. The dimensionless parameter that best quantifies a droplet's susceptibility to drift is the Stokes number [30] (S_{tk}):

$$S_{tk} = \frac{\tau_d}{\tau_\Lambda} = \frac{\rho_d d^2}{18\mu_g} \cdot \frac{C_\tau \varepsilon}{k} \quad (2)$$

Here, τ_d is the particle inertia time scale and τ_Λ is the turbulent integral time scale. When $St_k < 1$, droplet inertia relaxes faster than the flow time scale and droplets tend to follow streamlines, making them more susceptible to turbulent deflection. For $St_k > 1$, inertia dominates and droplet motion becomes more ballistic with reduced sensitivity to

airflow fluctuations. Accordingly, St_k serves as the core dimensionless parameter for characterizing drift susceptibility and is directly embedded in Lagrangian stochastic trajectory models [31].

Recent studies have also examined the differences of St_k calculations. Li et al. [32] compared multiple literature definitions and proposed a robust formulation for pressure and twin-fluid atomizers. They reported that at gas velocities above 10 m/s, $St_k < 0.1$ corresponds to droplet sizes of approximately 2–10 μm. Drift also depends on operating and meteorological conditions. Fattahi and Pour [33] used neural network sensitivity analysis and found that wind speed made the largest contribution to drift in their model (42%), followed by spray pressure (27%) and boom height (16%). These variables affect characteristic flow velocity, initial droplet-size distributions, and transport time. Ye et al. [34] experimentally studied airless spraying and found that ambient wind and spray height interact in their effects on droplet distribution.

Current drift-reduction strategies mainly follow two routes: nozzle-based approaches that modify flow development and droplet formation, and formulation-based approaches that alter fluid properties and atomization behavior. Among nozzle-based approaches, air-induction nozzles incorporate a Venturi passage that entrains air into the liquid stream, producing a gas–liquid two-phase flow in which the liquid sheet contains numerous microbubbles. Bubble growth and perforation are associated with local pressure gradients and Rayleigh–Taylor instability acting on the curved bubble interfaces [35]. Gong et al. [36,37] found that nozzle geometry affected bubble perforation. In their tests, enlarging the pre-orifice diameter and exit area increased the airflow rate by 701% and the liquid-sheet thickness by 312.5%, whereas increasing pressure mainly affected bubble size. These changes affected sheet breakup and the resulting droplet spectrum. Figure 3 shows the liquid sheet disintegration characteristics of spray sheets for air-induction nozzle.

Formulation-based regulation can reduce drift by changing the physicochemical properties of the spray liquid. Spanoghe et al. [38] noted that reducing surface tension alone often produces finer droplets, whereas increasing viscosity generally shifts the droplet spectrum toward larger sizes. Emulsified oil-based adjuvants can further increase droplet size. Lewis et al. [39] examined polymeric drift-control adjuvants (DCAs) and found that they increased jet extensional viscosity and resistance to breakup. Electrostatic spraying (Section 3.1.2) may also reduce drift by improving target-directed deposition through electric-field forces.

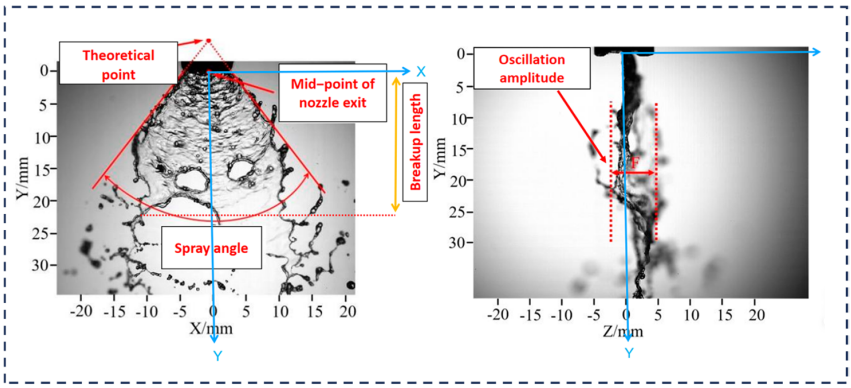


Figure 3. Spray sheets for air−induction nozzle [40].

3.1.2. Canopy Penetration: Air-Assisted and Electrostatic Spraying

(1) Air-Assisted Systems: Airflow-Driven Canopy Penetration

Air-assisted spraying improves canopy penetration by coupling droplet transport with a directed airflow field. Its effectiveness depends on airflow velocity, droplet size, canopy

structure, and leaf motion. Wu et al. [41] showed that airflow can induce large-amplitude leaf vibration under specific velocity and leaf-orientation conditions, showing that foliage motion can affect droplet deposition. Zhou et al. [42] reported that canopy geometry affects airflow penetration through drag and turbulent diffusion, linking spray penetration to leaf density and spatial arrangement. Comparative studies by Sánchez-Fernández et al. [43,44] showed that the rotor wake exhibits concentrated vertical momentum flux, promoting penetration into canopy gaps. However, in low-stature crops such as vineyards, ground confinement induces outward radial flow, increasing lateral drift risk. When flight height is comparable to canopy height, wake impingement on the ground leads to outward deflection and a ground-jet-like flow structure.

(2) Electrostatic Spraying: Charged-Droplet Deposition

Electrostatic spraying charges droplets through induction or contact, allowing electric forces to enhance deposition on abaxial surfaces and within the canopy. The electrostatic "wrap-around" effect can improve deposition efficiency under complex canopy geometries. He and Yang [45] showed that electrostatic charging reduced droplet size and narrowed the size distribution, while improving coverage uniformity on both adaxial and abaxial surfaces. Dong et al. [46] found that charging reduced off-target deflection and directed droplets toward leaf surfaces.

For aerial applications, droplet dynamics are influenced by the competition between electric stress, inertia, and surface tension, commonly described by the electric Euler number [47] $Eu_e = \epsilon_0 E^2/(\rho U^2)$ and the electric Weber number $We_e = \epsilon_0 E^2 d/\sigma$. A key limitation in electrostatic spraying is the tradeoff between atomization quality and charge-to-mass ratio (CMR). Li et al. [48] addressed these by developing a two-stage induction nozzle. At 12 kV, the CMR increased by 83.6%, and the volume median diameter (DV50) decreased by 23.6%. Two mechanisms may explain these changes. First, raising the applied voltage increases Eu_e: $Eu_e > 0.1$; in the cited study, $Eu_e > 0.1$ was associated with stronger electric effects on atomization, promoting finer droplets. Second, the maximum CMR occurs when the charge relaxation time $\tau_c = \epsilon/\sigma$ (where ϵ is permittivity and σ is electrical conductivity) matches the droplet transit time through the charging zone. At excessive voltage, corona discharge may occur, reducing charging efficiency and CMR [49]. Electrode material plays a crucial role in sustaining high CMR. Li et al. [50] related electrode Fermi level and work function to charge-transfer efficiency through the contact potential difference. Figure 4 presents the tower air-assisted spray test bench and two-stage induction-type electrostatic nozzle.

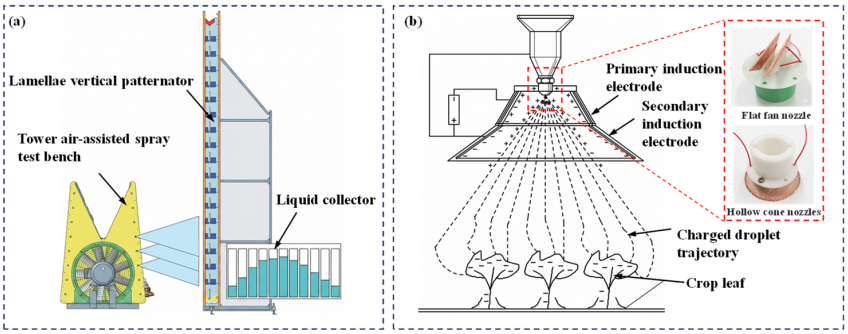


Figure 4. (**a**) Tower air-assisted spray test bench static liquid distribution measurement [42]; (**b**) working principle of the two-stage induction-type electrostatic nozzle [48].

(3) Multi-Technology Synergy and Intelligent Deposition Evaluation

Air-assisted and electrostatic spraying improve deposition through different but complementary mechanisms. Air-assisted spraying enhances convective droplet transport and

canopy penetration, whereas electrostatic spraying promotes target-directed motion of charged droplets through electric-field forces. Air assistance and electrostatic charging can also alter droplet-size and velocity distributions, and the resulting changes in droplet momentum may contribute to the observed deposition patterns. The two methods combine aerodynamic transport with electrostatic attraction within the canopy [51]. Field tests by Hu et al. [52] reported increases in deposition density of 34.9%, 30.4%, and 30.2% in the upper, middle, and lower canopy layers, respectively. These results show that the combined system increased deposition across all three canopy layers.

Dai et al. [53] used topology optimization to improve atomization and the charge-to-mass ratio of an air-assisted electrostatic nozzle. Appah et al. [54] noted that system performance depends on the electrical characteristics of both the droplets and target surfaces. For evaluation, traditional methods such as water-sensitive paper and manual counting are insufficient for high-throughput analysis. Dai et al. [55] developed an online sensor that records voltage increments proportional to deposited liquid mass.

Reported optimal parameter thresholds vary among crops and environmental conditions. Many numerical simulations use idealized steady wind and static canopy assumptions, which limits their representation of turbulent airflow and leaf motion. Systematic comparisons of air-assisted and electrostatic spraying under variable field conditions also remain limited.

3.2. Irrigation Trajectory: Spatial Water Distribution and Uniformity Evaluation

3.2.1. Hydraulic Parameters: Discharge Coefficient and Wet Radius

(1) Discharge Coefficient

The discharge coefficient (C_d) is defined as the ratio of actual to theoretical discharge and indicates how closely the actual discharge approaches the ideal value. The equation is expressed as:

$$C_d = \frac{Q_{actual}}{A\sqrt{2gH}} \tag{3}$$

where Q_{actual} denotes the measured discharge rate (m^3/s), A is the cross-sectional area of the nozzle exit (m^2), g is the acceleration of gravity (9.81 m/s^2), and H represents the working pressure head (m).

The discharge coefficient is affected by nozzle geometry and operating pressure. Zhu et al. [56] reported that in a complete fluidic sprinkler (CFS), increasing the contraction angle from 10° to 70° at 250 kPa reduced C_d from 0.90 to 0.67, which they attributed to increased flow resistance and energy loss associated with stronger separation. In contrast, rotating spray plate sprinklers (RSPSs) studied by Liu et al. [57] maintained $C_d > 0.90$ at pressures of 100–300 kPa for nozzle diameters of 2.98–3.77 mm. This suggests that smoother internal flow paths may reduce separation losses and help to maintain stable discharge.

Zhou et al. [58] established a power-law relationship for the internal pressure drop based on experimental data, using the Euler number $Eu = \Delta p/\left(\rho_L U_L^2\right)$. The Euler number expresses pressure loss relative to the flow dynamic pressure. Their model links pressure loss to variations in effective flow area, where reductions in area increase the loss coefficient and reduce the discharge coefficient. The model is valid for flow velocities of 0.5–2.5 m/s. For aerated impact sprinklers, Qureshi et al. [59] reported that a flow stabilizer increases exit velocity by 1.2% and reduces internal pressure loss by 28.4%, which they associated with lower turbulence intensity.

(2) Wet radius

Wet radius is the horizontal distance from the sprinkler center to the farthest droplet impact point under windless conditions. Li et al. [60] represented the wet radius for an

RSPS (rotating spray plate sprinkler), incorporating working pressure, nozzle diameter, installation height, and elevation angle:

$$R = f(p, d, h, \theta) \tag{4}$$

where p is the working pressure (kPa), d is the nozzle diameter (mm), h is the installation height (m), and θ is the elevation angle (°). The reported relative error was within 8%. Zhou et al. [61] derived a single-exponential model linking rotation speed and wet radius:

$$R = R_0 + A \cdot e^{(-\frac{n}{t})} \tag{5}$$

where R is the wet radius (m), n is the sprinkler rotation speed (r/min, revolutions per minute), and R_0 is the limit wet radius. Both A and t are constant coefficients calibrated from experimental data. The coefficients of determination (R^2) for this model consistently exceed 0.970, indicating a robust correlation. Their results showed that the influence of rotation speed on wet radius weakened above 20 r/min, whereas speeds below 4 r/min caused insufficient water distribution near the sprinkler. Liu et al. [62] developed a stochastic droplet motion model for CFS. The model accounts for aerodynamic drag when predicting droplet trajectories and spray range. It uses a gamma distribution for jet exit velocity and a uniform distribution for droplet deflection angle, reducing simulation error in average droplet diameter from 53% to 2%. Figure 5 describes the comparison of wet radius under different factor.

Many wet radius models are based on indoor windless conditions [63]. Dwomoh et al. [64] reported that natural wind altered sprinkler range. At a working pressure of 250–350 kPa, the outdoor downwind range can increase by 0.6–1.3 m, whereas the upwind range is decreased. Current models have limited applicability under outdoor windy conditions [65]. Future models should account for variable outdoor wind.

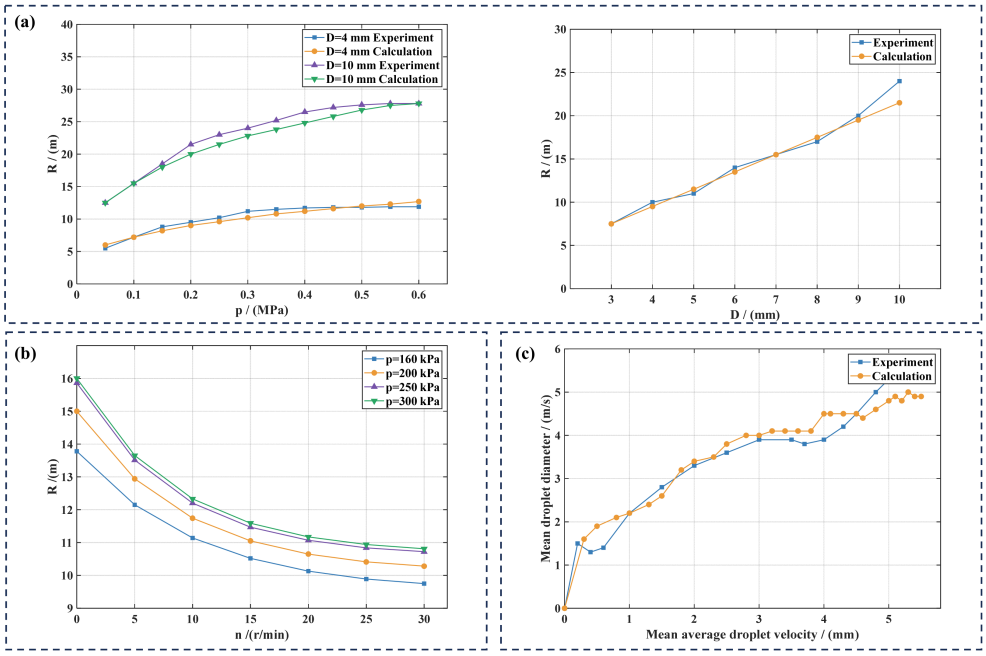


Figure 5. (**a**) Comparison between calculated and experimental wet radius under different factors (Li et al. [60]). (**b**) Relationship between rotational speed and wet radius (Zhou et al. [61]). (**c**) Droplet velocity with different droplet diameters (Liu et al. [62]).

3.2.2. Water Distribution Patterns and Modeling

The radial water distribution pattern describes sprinkler hydraulic performance. Different sprinkler structures produce distinct distribution shapes. Figure 6 shows the water distribution and Table 1 summarizes the distribution patterns reported by Zhu et al. [66] and subsequent studies.

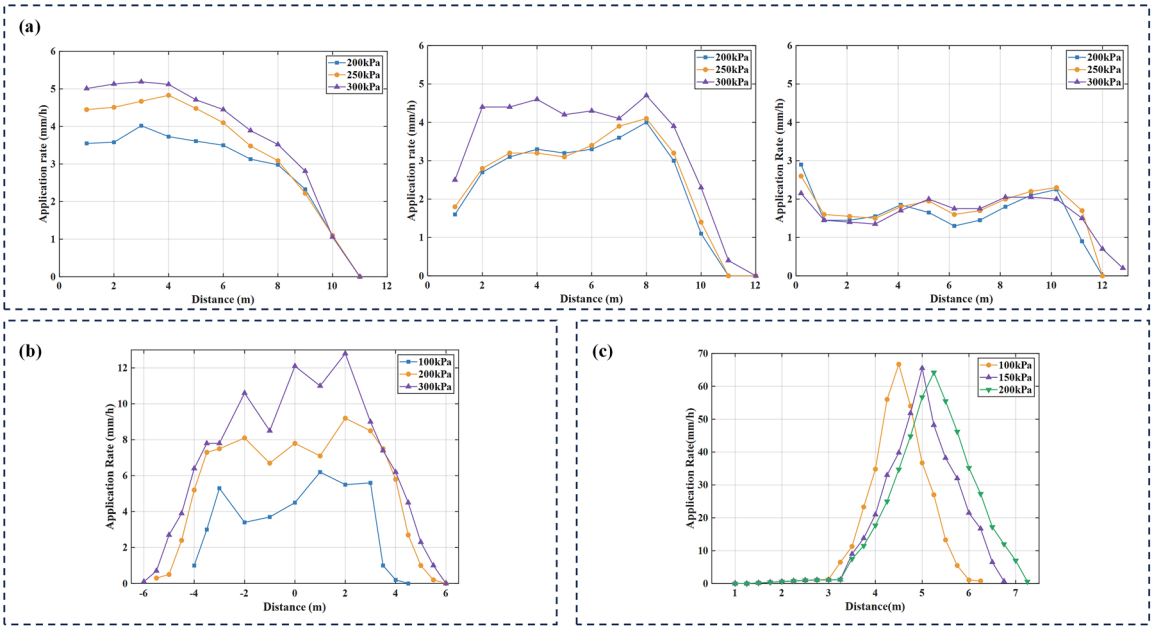


Figure 6. Water distribution (**a**) parabolic; elliptical; and saddle−shaped (Zhu et al. [66]). (**b**) Trapezoidal to parabolic evolution (Liu et al. [57]). (**c**) Triangular (Li et al. [67]).

Table 1. Water distribution patterns.

Sprinkler Type	Pattern	Formation Features
Outside signal fluidic sprinklers [66]	Parabolic	Peak application rate occurs at mid-to-far range, followed by a gradual decline.
Complete fluidic sprinklers [66]	Elliptical	Higher near-field deposition with a relatively flat mid-to-far region.
Impact sprinklers [66]	Saddle-shaped	Low near-field deposition, a pronounced mid-range peak, and rapid distal decay.
Rotating spray plate sprinklers [51]	Trapezoidal to parabolic	Approximately parabolic spray profiles were observed at 100–300 kPa, deviating from the commonly assumed trapezoidal distribution.
Non-rotating deflector sprinklers [60]	triangular	Peak deposition occurs at the distal region with limited near-field contribution.

These water distribution patterns [68] are sensitive to installation and operating conditions. Zhu et al. [69] demonstrated that under standard conditions (100–300 kPa working pressure and 1.5 m installation height), the local peak water volume is generally maintained at approximately 5.0 mm/h (standard deviation, $SD = 0.23$). However, lowering the installation height increased the peak application rate. For instance, at a constant pressure of 100 kPa, decreasing the installation height to 1.3 m and 1.1 m causes the peak intensities to surge to 8.9 mm/h and 10.5 mm/h, respectively. These results indicate that installation height and pressure should be considered when controlling local application peaks and

runoff risk. Fordjour et al. [70] reported that appropriate riser heights reduced airflow effects and improved sprinkler water distribution.

To describe radial distribution, empirical fitting models have been developed. Liu et al. [10] fitted the measured droplet-frequency distributions of a CFS using a lognormal distribution. A normalized lognormal probability density function is:

$$f(d) = \frac{1}{d\sigma\sqrt{2\pi}}\exp\left(-\frac{(lnd/d_max)^2}{2\sigma^2}\right) \quad (6)$$

where d denotes the droplet diameter (mm) and σ represents the standard deviation.

In addition to the lognormal function in Equation (6), normal and Rosin–Rammler (Weibull) functions are used to describe spray droplet-size distributions. The Rosin–Rammler function is commonly applied to cumulative volume distributions and characterizes the spectrum using a characteristic diameter and a spread parameter, whereas the lognormal function assumes that the logarithm of droplet diameter is normally distributed. Model suitability depends on the atomizer, operating conditions, weighting basis, and goodness of fit. For the complete fluidic sprinkler data summarized here, the cited study used the lognormal function because it satisfactorily represented the measured droplet-frequency distributions.

Indeed, for phenomena that are difficult to fit accurately using conventional functions, Zhou et al. [58] used Gaussian peak fitting in their study of swirling-straight sprinklers:

$$y = \frac{A_1 e^{\frac{-4\ln(2)(x-x_{c1})^2}{{\omega_1}^2}}}{\omega_1\sqrt{\frac{\pi}{4\ln(2)}}} + \frac{A_2 e^{\frac{-4\ln(2)(x-x_{c2})^2}{{\omega_2}^2}}}{\omega_2\sqrt{\frac{\pi}{4\ln(2)}}} + \frac{A_3 e^{\frac{-4\ln(2)(x-x_{c3})^2}{{\omega_3}^2}}}{\omega_3\sqrt{\frac{\pi}{4\ln(2)}}} \quad (7)$$

where y denotes fitting liquid level height in cm and A_i, ω_i and x_{ci} are fitting parameters. This study further revealed a significant linear correlation between the Gaussian fitting parameters and the internal pressure drop of the sprinkler.

The radial water distribution determines the local precipitation rate within the irrigated area. When precipitation exceeds soil infiltration capacity, runoff and erosion may occur [71]. Irrigation design aims to optimize sprinkler spacing and operating conditions to achieve uniform field-scale precipitation, which is evaluated using uniformity indices.

3.2.3. Uniformity Evaluation: Coefficient of Uniformity and Distribution Uniformity

(1) Coefficient of Uniformity

Christiansen's coefficient of uniformity (CU) is widely used to evaluate sprinkler water-distribution uniformity. Its value ranges from 0 to 100%, with higher values indicating a more uniform spatial water distribution [72]. The governing calculation formula is:

$$CU = \left(1 - \frac{\sum_{i=1}^{n}\left|h_i - \overline{h}\right|}{\sum_{i=1}^{n} h_i}\right) \times 100\% \quad (8)$$

where h_i is the water depth at each measurement point (mm), and $\overline{h}$ is the average water depth (mm).

Baiamonte and Vaccaro [73] proposed a normalized CU calculation method using numerical integration of the radial water distribution. The integration step, equivalent to the spatial sampling density, affects CU estimation accuracy; a step size of 13 points along the radius yields a relative error of about ±5%. Moreover, sprinkler spacing and layout format strongly impact the CU. Shi et al. [74] reported that when sprinkler spacing in a square layout increases from 1.0R to 1.4R, the combined CU decreased but remained

above 70%. A triangular layout at 1.4R produced a CU of 73.85%. Harmonic analysis coupled with the finite element method [75] has also been used to characterize uneven water distribution.

(2) Distribution Uniformity

Distribution uniformity (DU) serves as another prevalent uniformity evaluation metric, calculated as follows:

$$DU = \frac{\overline{h}_{low}}{\overline{h}} \times 100\% \quad (9)$$

where $\overline{h}_{low}$ is the average water depth of the lowest 25% of measurement points (mm), and $\overline{h}$ is the overall average water depth (mm). Unlike CU, DU emphasizes the lowest quarter of measured water depths and is therefore sensitive to under-irrigated areas. In the experiments of Zhu et al. [69], the standard deviation of DU across the 100–300 kPa pressure range was 15.5%, compared with 9.3% of CU.

Plant protection and irrigation both use droplet-trajectory models based on inertia, aerodynamic drag, and gravity, but their control objectives differ. Plant-protection studies use parameters such as the Stokes number to assess drift and examine electrostatic forces to improve canopy interception, while sprinkler irrigation focuses on wetted radius and uniform ground-level water distribution. Research in the two fields remains separate, and most empirical models are calibrated for specific emitters, operating conditions, and environments. Cross-domain models linking drift control with irrigation uniformity remain limited.

4. Device-Scale: Hydraulic Design and Structural Innovations of Sprayer

While the previous section explored the spatial distribution and target penetration of sprays, these outcomes are influenced by the hydraulic and geometric design of emitters. This section reviews the hydraulic characteristics and structural design of sprayers.

4.1. Nozzle Technologies for Plant Protection

Plant-protection nozzles affect spray atomization characteristics. For this review, nozzles are grouped by their main atomization or charging mechanism into three types: hydraulic nozzles [76], which rely on pressure-driven breakup of liquid jets or sheets; centrifugal nozzles [77,78], which employ high-speed rotation to thin and destabilize liquid films; and electrostatic nozzles, which apply electric forces to charged droplets to enhance target deposition.

4.1.1. Hydraulic Nozzles

Hydraulic nozzles are the most widely used type in agriculture. Driven by hydraulic pressure, liquid is forced through an orifice to form a sheet or jet, which then disintegrates into droplets due to hydrodynamic and aerodynamic instabilities. By modifying internal flow channels and exit geometries, these nozzles can generate different spray patterns and droplet sizes suitable for various application targets.

(1) Standard flat fan nozzles

Standard flat-fan nozzles use a converging slot to accelerate liquid into a thin, fan-shaped sheet. The slot geometry affects sheet thickness and spray angle [79]. At typical operating pressures (0.2–0.5 MPa), the turbulent flow produces a narrow droplet spectrum rich in fine droplets (V denotes droplet diameter, $V < 150$ μm) [80]. Owing to their low Stokes number, these fine droplets closely follow ambient air streamlines and exhibit high susceptibility to wind drift. Despite this limitation, the uniform sheet structure ensures

consistent coverage on the adaxial leaf surface. As Wang et al. [81] noted, standard flat-fan nozzles offer good uniformity but are unsuitable for wind-sensitive conditions.

(2) Air-induction nozzles

Air-induction nozzles minimize drift without compromising coverage [82]. They feature an inlet Venturi tube where high-velocity liquid creates negative pressure to entrain air, thereby forming a gas–liquid two-phase flow. Upon ejection, the resulting spray sheet contains numerous microbubbles. As the sheet breaks up, bubble rupture produces relatively coarse, air-filled droplets. Bench tests by Gil et al. [83] showed that the drift potential value (DPV) of Venturi flat fan nozzles is substantially lower than that of conventional XR 11003 nozzles, demonstrating relationships between microscopic droplet size parameters and macroscopic DPV (R^2 = 0.58–0.72). Yu et al. [84] evaluated the field efficacy of air-induction nozzles during aerial application trials on soybean and rice canopies. These nozzles achieved 2.3 times the effective coverage of conventional flat-fan nozzles. These results indicate that air-induction nozzles can reduce drift [85] while maintaining or improving effective coverage under specific application conditions.

(3) Hollow cone nozzles

Unlike flat-fan nozzles, hollow cone nozzles use an internal swirl core to generate strong centrifugal force, forming a hollow conical spray sheet at the exit. Farias et al. [86] verified that highly atomized droplets provide advantages for microscopic coverage of dense foliage, making them suitable for applications requiring complete wetting. Tangential grooves control swirl intensity, while interaction between the rotating liquid sheet and ambient air promotes breakup into fine droplets. However, this fine atomization significantly increases the risk of wind drift. Nuyttens et al. [87] reported that, under the tested conditions, hollow cone nozzles generate a significantly higher proportion of fine droplets ($V < 150$ μm, 50–70%) than flat-fan or air-induction nozzles, explaining their elevated drift risk. They are therefore often used in low-wind or short-distance applications (e.g., air-assisted orchard sprayers), where reduced travel distances limit drift and allow their superior coverage and penetration capabilities to be utilized effectively.

4.1.2. Centrifugal Nozzles

Unlike pressure-driven hydraulic nozzles, centrifugal nozzles use a high-speed rotating disc or cup to atomize liquid via centrifugal force. Droplet size is primarily determined by rotational speed and liquid feed rate. At a constant feed rate, increasing rotational speed reduces liquid-film thickness at the disc edge, thereby promoting finer atomization. The overall droplet spectrum also depends on liquid viscosity and surface tension. In field applications, auxiliary airflow [88] has a significant influence on the transport and deposition of centrifugally generated droplets. Bayat and Bozdogan [89] systematically evaluated in a wind tunnel how disc rotational speed, auxiliary air velocity, and application rate influence drift potential. Finer droplets produced at high rotational speed have a smaller Stokes number, making them more prone to follow air streamlines and thus more drift-prone under crosswind conditions. Yao et al. [90] evaluated centrifugal spraying across various crops and found that higher spray volumes increased overall canopy deposition but also intensified spatial heterogeneity. This phenomenon occurs because increased flow rates increase liquid-film thickness on the disc and broaden the droplet-size distribution. Consequently, fine droplets are easily scattered by rotor downwash, whereas coarse droplets penetrate deeper but cause localized over-deposition.

4.1.3. Electrostatic Nozzles

Electrostatic nozzles are mainly classified into induction-charging and contact-charging types. By imparting electrical charges to droplets, electrostatic spraying technology can significantly improve droplet uniformity and reduce spray drift [91,92]. Targeting long-distance air-assisted spraying in greenhouses, Lin et al. [93] developed a waist-shaped charging device to replace conventional circular electrodes. The waist geometry alters the electric field lines: the smaller radius of curvature in the spray direction concentrates the field in the waist region. This configuration locally increases the electric Euler number and generates stronger lateral deflection forces on charged droplets, thereby improving radial distribution uniformity (CV decreased from 33.7% to 17.9%). Ou et al. [94] designed an air-assisted electrostatic spraying system based on transverse jet atomization. Single-sided spraying trials demonstrated that electrostatic effects enhanced droplet deposition within the canopy and on abaxial leaf surfaces. However, at extended distances, strong electrostatic attraction may cause premature droplet interception by outer leaves, thereby limiting penetration into deeper canopy regions. Working distance should be selected to balance abaxial coverage and canopy penetration.

Table 2 compares the atomization mechanisms, major advantages, and inherent limitations of contemporary plant-protection nozzles. The comparison indicates that nozzle selection requires balancing atomization performance, drift mitigation, canopy coverage, and deposition uniformity.

Table 2. Classification and characteristics comparison of plant-protection nozzles.

Nozzle Classification	Operational Principle	Representative Metrics	Typical Use	Advantages and Limitations
Standard flat fan	Pressure-driven breakup of a liquid sheet	Operating pressure: 0.2–0.5 MPa; $D_{V0.5}$: 150–250 μm	Field herbicide and insecticide spraying	Low cost and uniform fan pattern; high fine-droplet drift risk
Air induction	Venturi air entrainment and breakup of an aerated liquid sheet	$D_{V0.5}$: 300–450 μm; effective coverage was 2.3 times that of conventional flat-fan nozzles in the cited soybean and rice trials	Herbicide spraying, drift-sensitive conditions, and UAV application	Lower drift; coarse droplets may reduce surface coverage
Hollow cone	Swirl-induced breakup of a conical liquid sheet	$D_{V0.5}$: 80–150 μm; droplets smaller than 150 μm accounted for 50–70% under the tested conditions	Fungicide, orchard, and dense-canopy spraying	High coverage and canopy penetration; high drift and clogging risk; shorter range
Centrifugal	Breakup of a liquid film from a rotating disc or cup	Droplet size: 100–250 μm; droplet size varies with rotational speed and liquid flow rate	UAV spraying	Adjustable droplet size; requires a motor; deposition may be uneven over wide swaths
Electrostatic	Induction or contact charging of spray droplets	At 12 kV, CMR increased by 83.6% and DV50 decreased by 23.6% in a two-stage induction nozzle; radial CV decreased from 33.7% to 17.9% in the cited greenhouse test	UAV and greenhouse pesticide spraying	Improved target deposition; performance declines with charge decay and high humidity

Comparative nozzle performance depends on application conditions. Reported optimal operating pressures and anti-drift thresholds vary among studies because of differences

in testing wind speeds, crop canopy structures, and spray formulations. Many studies use controlled or flat-field conditions that do not fully represent field turbulence and canopy motion. Few studies optimize drift control, penetration depth, and deposition uniformity together.

4.2. Sprinkler Technologies for Irrigation

Hydraulic sprinklers [95] affect irrigation quality, energy consumption, and water-use efficiency [96]. Rising energy costs and demand for water conservation have encouraged the development of low-pressure irrigation [97]. Recent sprinkler designs aim to maintain adequate throw radius, distribution uniformity, and droplet characteristics while operating at reduced pressures.

4.2.1. Impact Sprinkler

The impact sprinkler (IS) converts the kinetic energy of the water jet into intermittent rotation through an oscillating arm (Figure 7a). This drive mechanism requires sufficient jet momentum to overcome arm inertia and friction. When the operating pressure falls below about 200 kPa, the jet velocity and impact force decrease, causing incomplete or unstable arm motion. This can cause irregular rotation and lower water distribution uniformity [98,99].

To improve low-pressure performance, the aeration impact sprinkler (AIS) entrains air at the nozzle and converts the single-phase jet into a gas–liquid two-phase flow [11]. Qureshi et al. [59] optimized the AIS internal channel using CFD and introduced a flow stabilizer. Air entrainment introduces bubbles and disturbances into the jet, promoting jet breakup at reduced pressures. The stabilizer smoothed the velocity profile, suppressed large-scale vortices, and reduced turbulent kinetic energy below 1.0 m^2/s^2. The optimized design increased exit velocity by 1.2% and decreased pressure loss by 28.4%, indicating that controlling internal flow separation and turbulence can improve hydraulic efficiency.

Another modification is the installation of a fixed water dispersion device on the IS [100,101]. This device, usually a perforated plate or deflector, intercepts the jet and spreads it into a wider spray. Its insertion depth affects the degree of jet impingement, dispersion angle, and energy loss. Li et al. [102] showed that deeper insertion increases jet obstruction but also causes greater energy dissipation. Issaka et al. [103] reported that an IS equipped with a C2 dispersion device achieved a uniformity coefficient of 86.67% at 200 kPa. C2 denotes a pointed-tip fixed water dispersion device with a device diameter $D = 8$ mm, a jet-impact impact angle $\theta = 45^\circ$, and a penetration depth $d = 4.0$ mm. This device converts a concentrated high-speed jet into a wider, lower-speed spray, lowers peak application rate, and improves water distribution uniformity.

4.2.2. Fluidic Sprinkler

The complete fluidic sprinkler (CFS) replaces mechanical drive with fluidic control based on the Coanda effect [104] (Figure 7b). Its rotation depends on stable jet attachment, detachment, and switching inside the fluidic element. When operating pressure falls below approximately 200 kPa, both jet momentum and the pressure difference between the attachment and opposite sides are reduced. The weakened control flow may fail to detach the jet or trigger unstable switching, leading to intermittent rotation and reduced distribution uniformity. Zhu et al. [105] reported a uniformity coefficient of only 78% at 150 kPa. This result indicates that low-pressure operation can weaken switching stability in this configuration.

Low-pressure performance depends on the geometry of the fluidic element [106]. Nozzle diameter determines jet momentum, wall length controls attachment stability, and control-port design affects signal-switching efficiency. The dynamic fluidic sprinkler

(DFS) was developed by modifying these parameters to improve low-pressure operation, rather than significantly reducing the operating pressure without compromising spray uniformity. Fordjour et al. [107] showed through CFD that tube length controls signal-flow transmission time, tube diameter affects pressure loss, and nozzle diameter determines jet momentum. With a 5.5 mm nozzle at 150 kPa, the DFS achieved a uniformity coefficient of 86%, higher than the 78% of the CFS under the same condition [105,108,109]. This demonstrates that optimizing internal flow paths can stabilize jet switching and improve low-pressure irrigation performance.

The outside-signal (OS) fluidic sprinkler is another key structural variant. Unlike the CFS, the OS channels the signal flow externally and employs a dual-nozzle configuration [110]. The main nozzle produces the primary jet that drives rotation, while a smaller auxiliary nozzle generates a control jet that is fed externally to the fluidic element. The angle of the auxiliary nozzle relative to the main jet affects the interaction between the two jets. Jiang et al. [111] found that when the auxiliary nozzle elevation angle is set to 34.5°, the two jets interact optimally. At this angle, the auxiliary jet strikes the main jet at an oblique angle. The collision generates shear layers and local vorticity, which dissipate part of the momentum of the main jet.

4.2.3. Plate Sprinklers

Rotating spray plate sprinklers (RSPSs) present an alternative for low-pressure irrigation (Figure 7c). Unlike Coanda-based fluidic designs, RSPS rotation is driven by the impact torque of a jet striking a grooved plate, giving them relatively stable operation under low-pressure conditions. Sourell et al. [112] verified that RSPS configurations maintain a combined uniformity exceeding 93% at an operating pressure as low as 200 kPa. The rotating grooves shear the jet into droplets, whose size depends on the groove geometry (depth, width, and angle) and the relative velocity between the jet and the plate.

The fixed spray plate sprinkler (FSPS) uses a stationary grooved plate. Zhao et al. [113] systematically optimized three geometric parameters: the number of grooves (m), the deflector angle (α), and the groove inclination angle (β). These parameters control how the jet is split and deflected. At 0.1 MPa, their optimal configuration (m = 22, α = 42°, β = 11°) increased the wet radius by 5.45% and reduced the peak application rate by 68.14%. This reduction can limit local water accumulation. However, Liu et al. [57] found that, although the RSPS discharge coefficient exceeded 0.9, its water distribution pattern remained sensitive to variations in nozzle diameter and operating pressure.

4.2.4. Rotating Sprinklers

Rotating sprinklers (RSs) (Figure 7d) are used in modern solid-set systems and on sloping fields because of their compact structure, adjustable throw radius, and high water distribution uniformity. Issaka et al. [114] compared rotating sprinklers equipped with rotating dispersion devices against impact sprinklers equipped with fixed dispersion devices. Their study found that rotation speed varied among quadrants. The authors associated this alternating motion with greater wind resistance and better filling of gaps in water distribution, although their water distribution deviation remains slightly higher than that of impact sprinklers.

Operating pressure is a major factor affecting rotating sprinkler performance. Li et al. [115] found that applying trapezoidal dynamic pressure to a Hunter MP2000 sprinkler increased the CU to 93.20%. This approach also expanded the wetted area by 39.67% and reduced the average application rate by 8.62%, indicating that dynamic pressure can compensate for local water deficits under the tested conditions. Hua et al. [116] developed a 3D computational model coupling droplet trajectory, the WAVE (Kelvin–Helmholtz)

secondary-breakup model, and water application superposition. Their analysis identified an exponential relationship between droplet velocity and diameter and a logarithmic correlation relationship between droplet diameter and spray distance. The model can support structural optimization and performance prediction.

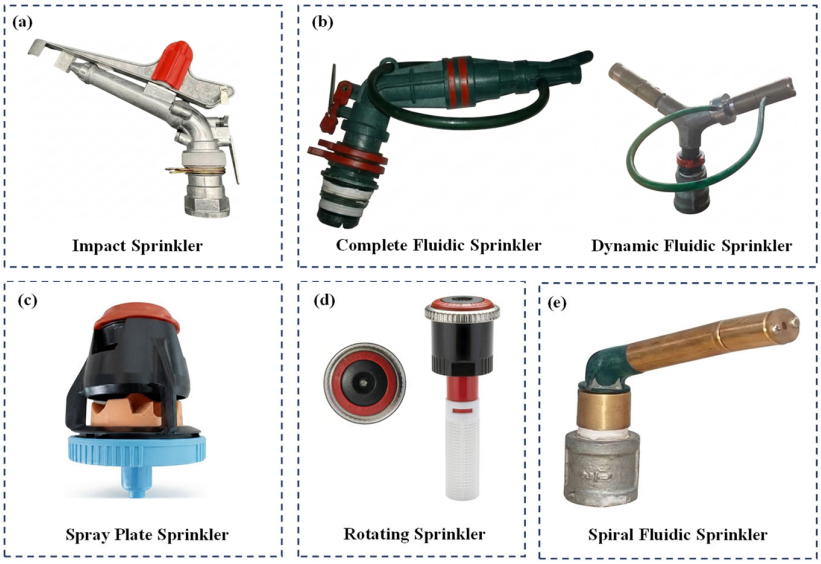


Figure 7. Sprinklers used in irrigation studies. (**a**) Impact sprinkler; (**b**) Fluidic Sprinkler; (**c**) Plate Sprinklers; (**d**) Rotating Sprinklers; (**e**) Spiral Fluidic Sprinkle [77,115,117–119].

4.2.5. Spiral Fluidic Sprinkler

The spiral fluidic sprinkler (SFS) is a recent design (Figure 7e). Unlike straight-channel fluidic sprinklers relying primarily on aerodynamic drag for droplet breakup during wall attachment, the SFS imparts a swirling motion to the fluid before discharge. This mechanism increases turbulence intensity and promotes droplet breakup. Lewballah et al. [117] reported that, at 200 kPa with a 4 mm nozzle, the SFS exhibited a coefficient of variation of 6.2%, with more than 90% of the droplets smaller than 3 mm in diameter.

The classification system and technical characteristic comparison of the sprinklers is shown in Table 3.

Table 3. Classification system and technical characteristics comparison of irrigation sprinklers.

Type	Driving Principle	Pressure Sensitivity	Representative Result	Advantage	Limitations
IS	Water jet acting on an oscillating arm	High	CU = 86.67% at 200 kPa with C2	Mature and reliable	Unstable rotation at low pressure
AIS	Jet impact combined with air entrainment	Medium	Exit velocity +1.2%; pressure loss −28.4%	Improved breakup at reduced pressure	Complex internal flow
CFS	Coanda attachment and jet switching	Medium	CU = 78% at 150 kPa	No mechanical drive	Unstable switching at low pressure
DFS	Modified fluidic element and signal-flow control	Low	CU = 86% at 150 kPa with a 5.5 mm nozzle	Improved low-pressure operation	Sensitive to internal geometry
OS	External signal flow with a dual-nozzle arrangement	Medium	Auxiliary-nozzle angle = 34.5°	Controllable jet interaction	Complex nozzle arrangement

Table 3. *Cont.*

Type	Driving Principle	Pressure Sensitivity	Representative Result	Advantage	Limitations
RSPS	Water jet acting on a rotating grooved plate	Low	Combined $CU > 93\%$ at 200 kPa	Stable low-pressure operation	Distribution varies with nozzle and pressure
FSPS	Water jet acting on a stationary grooved plate	Low	At 100 kPa: wetted radius +5.45%; peak rate −68.14%	Lower local application peaks	Distribution depends on groove geometry
RS	Internal rotational driving	Low	Dynamic pressure: $CU = 93.20\%$; wetted area +39.67%; mean rate −8.62%	Adjustable range and high CU	Quadrant-to-quadrant variation
SFS	Spiral flow channel	Low	At 200 kPa with a 4 mm nozzle: $CV = 6.2\%$; >90% of droplets < 3 mm	Improved low-pressure breakup	Limited validation

4.3. Influencing Factors of Hydraulic Regulation

4.3.1. Effect of Operating Pressure

Operating pressure affects jet exit velocity and therefore spray range. Hussain et al. [120] found that increasing the operating pressure from 100 to 250 kPa increased the spray range of the R3000 RSPS. The impact of pressure on spray range heavily depends on the sprinkler's discharge mode and structural design. In a systematic review, Dwomoh et al. [121] reported that complete fluidic sprinklers are mechanically simple and support low-pressure operation. However, at comparable pressures of 200–350 kPa, they converted jet kinetic energy into spray range less effectively than traditional impact sprinklers and showed greater spatial variability in application rate.

Recent studies have also used pressure regulation to switch between irrigation and pesticide application modes. Liu et al. [122] innovatively developed a pressure-self-controlled water-pesticide integrated sprinkler. Utilizing particle image velocimetry (PIV) and a 2D video disdrometer (2DVD), they confirmed that stepwise pressure switching can fundamentally transform the system's spray paradigm. At lower pressure, the sprinkler produced coarser droplets with lower transport velocity, suitable for root-zone irrigation. When pressure increased to 400 kPa, the jet produced finer droplets with improved canopy penetration potential.

In contrast, increasing operating pressure creates a distinct tradeoff. Although higher pressures improve atomization, they significantly increase the proportion of drift-prone fine droplets. Pressure should therefore be selected according to the application: irrigation may use higher pressure to extend spray range, whereas pesticide spraying must avoid pressures that generate excessive drift-prone droplets.

4.3.2. Effect of Structure Parameters

The internal flow channel dictates fluid dynamics at the nozzle exit, where even minor structural changes can significantly alter overall hydraulic performance. Consequently, adopting non-circular nozzle designs effectively reduces localized peak application rates.

Investigations by Jiang et al. [14] on IS confirmed that under low-pressure conditions of 150–200 kPa, adopting non-circular cross-section nozzles, such as elliptical or rhombic configurations, can precipitate early jet instability and generate coarser mass-weighted droplets. A comparative study by Chen et al. [123] further indicated that although circular nozzles exhibit greater potential for extending the spray range, non-circular nozzles are

more conducive to achieving high-uniformity coverage under low-pressure operations. Concerning flat fan nozzles, Mughal et al. [124] discovered that the depth of the V-cut at the nozzle edge directly controls the spanwise lateral diffusion of the jet; a deeper cut correlates with a broader spray angle and an enhanced degree of droplet atomization. Figure 8 shows the sprinkler with different nozzles.

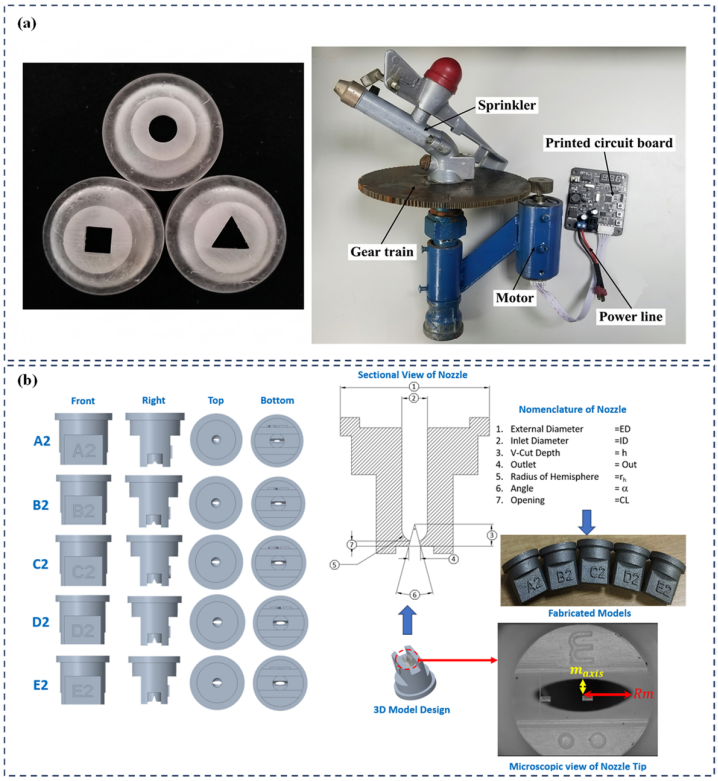


Figure 8. (**a**) Sprinkler with different nozzles (Lin et al. [125]). (**b**) Different V-cut depth of flat-fan nozzle (Mughal et al. [124]).

The dimension of the nozzle orifice dictates the baseline flow rate and hydraulic load of the jet. Hussain et al. [120] indicated that when the nozzle diameter is doubled from 3.18 mm to 6.35 mm, the system's hydraulic load scales exponentially. The velocity–droplet diameter relationship presents an exponential trend: tiny droplets experience strong air drag and decelerate sharply, while large droplets retain higher flight speed with minor velocity loss, forming a typical exponential decay curve. In the context of precise micro-dimensional calibration, Wu et al. [126] found that under the unstable pumping conditions of photovoltaic water-pumping irrigation systems, a circular combined nozzle featuring a cross-sectional area of 7 mm^2 and a straight channel length of 2 mm yields the most highly consistent flow velocity field.

Plant-protection nozzles and irrigation sprinklers follow similar atomization principles based on liquid jet fragmentation, yet their structural optimization targets differ substantially in existing research. Pesticide nozzle design prioritizes adjusting internal channels and charging components to suppress fine droplet drift and boost leaf capture, while irrigation emitter innovations focus on jet breakup structures, rotating mechanisms and flow stabilizers to extend wet radius and homogenize ground water distribution. Existing structural improvement strategies are mostly developed for either anti-drift spraying or uniform irrigation. Limited efforts explore cross-domain design references and generalized structural optimization principles applicable to both agricultural spray scenarios.

5. System-Scale: Energy-Saving Design and Intelligent Control

Although previous sections have discussed droplet physics, transport dynamics, and hardware design, these emitters ultimately function as terminal components within broader agricultural systems. Accordingly, this section examines system-level developments in spraying and irrigation equipment, with emphasis on how pressure–flow regulation controls spray formation and water distribution.

5.1. Energy Consumption Analysis and Conservation Regulation

5.1.1. Energy Consumption Composition

The energy consumption of sprinkler irrigation systems mainly arises from three fluid-related processes: pump work input, pressure losses in the pipe network, and jet atomization at the sprinkler outlet.

The pumping unit is the primary energy-consuming component and typically accounts for more than 70% of the total energy consumption. Tarjuelo et al. [127] pointed out that during irrigation district modernization, energy consumption often increases nonlinearly with increasing operating pressure. To address this issue, variable frequency drive (VFD) technology has increasingly replaced conventional valve-throttling methods. Within the fluid network, localized hydraulic resistance causes irreversible pressure losses and associated energy dissipation [128]. Chen et al. [129] developed an adaptive pressure–flow regulator. By utilizing an internal elastic diaphragm to dampen pressure spikes, this device ensures a steady flow rate at terminal sprinklers despite upstream instability, effectively reducing excess energy consumption.

Terminal operating pressure directly determines sprinkler energy consumption. Early research by Topak et al. [130] confirmed that low-pressure sprinklers (150–200 kPa) can reduce energy consumption by 25–35% compared with conventional high-pressure models (300–400 kPa). However, excessive pressure reduction does not necessarily result in optimal energy efficiency. Experiments by Chen et al. [23] revealed that when the pressure drops below a critical 100 kPa threshold, the jet's deficit in initial kinetic energy severely hampers the aerodynamic breakup process. A study by Dwomoh et al. [121] further indicated that although structurally simplified fluidic sprinklers reduce pump demand under low-pressure conditions, this benefit is achieved at the expense of spatial distribution performance. This physical tradeoff results in a 9.3–11.0% decrease in wet radius and increased spatial variability in application rates.

In UAV plant protection, the energy bottleneck differs from that of conventional irrigation systems. It is governed less by fluid transport than by the tradeoff between aerodynamic power consumption and spray payload. Optimizing flight trajectories and coordinating flight velocity with spray flow rate are essential for improving UAV operational energy efficiency [131].

5.1.2. Regulation for Energy Conservation

Achieving system-level energy conservation requires integrating hydraulic performance assessments with dynamic control.

Zhu et al. [132] showed that Low Elevation Spray Application (LESA), through reduced sprinkler height, optimized spacing, and adjusted travel speed, achieved irrigation uniformity of up to 96.4% while operating at reduced pressure. Mohamed et al. [73] further noted that small-scale spatial non-uniformity below 30 cm can be partially compensated by soil-water redistribution and root uptake. Adoption of this evaluation framework increased the uniformity index by 3–8% and reduced compensatory irrigation volumes by 9–12.5%. Zhang et al. [133] demonstrated that intermittent pulsed spraying improved uniformity by 11.7–20.1%, while reducing peak application rates and runoff risks. Hui et al. [134] also

found that rotating spray plate sprinklers provide better application accuracy than fixed-plate sprinklers under variable-rate irrigation. These studies indicate that effective energy conservation requires more than simply reducing pressure; it involves coordinated regulation of pressure, sprinkler configuration, travel speed, and application-rate distribution.

5.2. Data-Driven Approaches in Performance Prediction

5.2.1. Application of Machine Learning

Driven by advances in artificial intelligence and big data technologies, sprayer and sprinkler design is shifting from empirical trial-and-error approaches toward data-driven optimization. Traditional hydraulic assessments rely heavily on semiempirical formulas and computationally intensive physical models, which fail to capture the nonlinear mechanisms of multi-parameter coupling. In contrast, machine-learning (ML) techniques [135–137] excel at extracting hidden patterns from massive experimental or simulation datasets to construct highly accurate surrogate models [27]. Owing to their strong nonlinear fitting capabilities, ML algorithms have increasingly replaced conventional statistical models and become important tools for predicting system performance.

Early predictive efforts predominantly utilized Multiple Linear Regression (MLR) [138]; however, this approach produced considerable errors when modeling complex nonlinear hydraulic responses. Skhiri et al. [139] demonstrated that under multivariate inputs, Artificial Neural Networks comprehensively outperform MLR models in predicting the uniformity coefficient. Menezes et al. [140] formulated a neuro-computing model based on a Multilayer Perceptron that utilizes field spatial coordinates (x, y) as input features to directly predict the spatial water distribution patterns of a single sprinkler, achieving a coefficient of determination of 0.9085. Regarding network topology selection, Hu et al. [141] comparatively evaluated the predictive capacities of BP and RBF neural networks for predicting the wet radius of fluidic sprinklers. Their results showed that although both architectures captured the nonlinear relationship between wet radius and operating pressure, the RBF network demonstrated superior engineering applicability in terms of training stability and prediction accuracy. Within the range covered by the training data, the predicted water distribution, wet radius, and uniformity can be used to screen sprinkler structures, operating pressures, and spacing configurations before physical testing. This approach reduces experimental workload and assists in selecting field layouts and operating conditions, although final designs still require experimental verification.

As input variables (e.g., wind speed, temperature, humidity, and installation height) increase in number, individual neural networks become susceptible to overfitting. Therefore, ensemble learning algorithms, particularly Random Forest (RF) [142] and extreme gradient boosting (XGBoost) [143], have become widely adopted approaches. Elhussiny et al. [144] developed high-precision predictive frameworks encompassing RF, XGB, and a hybrid architecture (XGB-RF), demonstrating that the hybrid model achieved R^2 values above 0.82 for predicting DU and CUC. In evaluating rotating spray plate sprinklers, Hussain et al. [145] applied four machine-learning algorithms for high-throughput prediction and found that XGB achieved the lowest RMSE for CUC prediction (1.79%), whereas RF performed better in predicting droplet diameter (DD).

Machine learning has been increasingly applied in UAV-based pesticide spraying systems [146]. Mowla et al. [147] emphasized that conventional ML methods remain effective for moderate-sized datasets and applications requiring interpretability. Focusing on spray performance, Wang et al. [148] developed an economical autonomous spraying system driven by a Regression Forest model. By dynamically regulating spraying operations, this system maintained the variation coefficient below 30% and improved application accuracy.

5.2.2. Application of Optimization Algorithms

After establishing performance prediction models, identifying optimal structural parameters becomes essential for further hardware development. Currently, parameter optimization in sprinkler irrigation is evolving from discrete parameter screening toward global multi-objective optimization strategies [149].

Orthogonal experimental design [150] remains a foundational tool for structural parameter optimization, proving adept at delineating primary and secondary factors during nascent design phases. By deploying a four-factor, three-level orthogonal array to assess low-pressure LESA technology, Zhu et al. [132] successfully isolated machine travel speed and nozzle diameter as the predominant variables dictating surface runoff. Similarly, utilizing range analysis, Wu et al. [126] pinpointed the optimal geometric configuration for photovoltaic irrigation sprinklers (a circular outlet, a 7 mm^2 area, and a 2 mm flow channel length). This geometric arrangement fundamentally curtails internal hydraulic energy dissipation, thereby markedly bolstering rotational stability and radial water distribution under low-pressure regimes.

Whereas orthogonal experiments are limited to comparisons across discrete parameter nodes, response surface methodology (RSM) [151] elucidates nonlinear interactive effects by mapping continuous mathematical surfaces. Applying RSM for multi-objective optimization of FSPS deflectors, Zhao et al. [113] quantified the independent effect of groove count on peak application rates. At a reduced pressure of 0.1 MPa, the optimized prototype improved CU and the coefficient of uniformity for fertigation (CUF) by 20.06% and 31.02%, respectively. In a parallel effort, Chen et al. [23] applied RSM to determine the optimal combination of nozzle diameter and spray plate geometry for low-pressure rotating sprinklers, thereby addressing the uniformity limitations associated with low-pressure operation.

Genetic algorithms (GAs) [152] have been used to identify Pareto optimal design solutions. Kim [153] applied a micro-genetic algorithm to optimize sprinkler water-flux distribution and enhance droplet spatial uniformity. More recently, data-driven optimization combined with physical simulations has emerged as an effective strategy for sprinkler design. Pan et al. [154] and Li et al. [155] integrated RF-NSGA II with CFD simulations to optimize an intermittent water-dispersing pin sprinkler. The surrogate model rapidly identified Pareto-optimal parameters, whereas CFD analysis revealed the underlying hydraulic mechanisms. The optimized structure extended wet radius and expanded liquid-film distribution, thereby compensating for uniformity degradation.

Despite the high prediction accuracy of traditional machine-learning algorithms, they possess notable inherent limitations. Their performance strongly depends on the completeness and coverage of training datasets, which may result in unreliable extrapolation beyond the range of available experimental conditions. Most black-box models lack physical interpretability and are unable to quantitatively evaluate prediction uncertainty, thereby limiting their practical deployment in field applications. To overcome these limitations, physics-informed machine learning (PIML), which incorporates droplet dynamics and hydraulic governing equations into model training, has emerged as a promising approach that combines data-driven learning with physical constraints to enhance model generalization and interpretability.

Energy-saving and intelligent control strategies in both plant-protection UAV spraying and ground sprinkler irrigation systems increasingly rely on similar data-driven frameworks. Irrigation system optimization mainly focuses on reducing pumping losses and balancing low-pressure operation with distribution uniformity, whereas intelligent regulation in pesticide spraying emphasizes flight energy consumption and crosswind drift mitigation. Machine learning, response surface methodology, and genetic algorithms are widely used analytical tools in both fields. In addition, most existing optimization cases

adopt static offline parameter tuning under fixed meteorological and crop conditions. Comparative evaluations among different optimization algorithms remain inconsistent across the literature. A general consensus has not yet been established regarding evaluation criteria for convergence efficiency and robustness.

However, existing algorithmic frameworks and control strategies have largely evolved independently within each discipline. Few studies have explored the transfer of mature intelligent control strategies between irrigation and plant-protection systems, and limited efforts have been devoted to developing generalized system-level optimization platforms for multifunctional agricultural spraying equipment.

6. Conclusions and Future Perspectives

6.1. Conclusions

This review comparatively analyzes plant protection and sprinkler irrigation systems from a multi-scale fluid-application perspective. Through analysis at the microscopic (droplet), macroscopic (spray), equipment, and system scales, the review highlights the shared fluid-dynamic basis and the different engineering objectives of these two fields. The principal conclusions are as follows:

- Although pesticide application and sprinkler irrigation rely on similar liquid breakup and droplet transport mechanisms, their target interaction requirements differ substantially. Plant protection focuses on reducing drift, improving canopy penetration, and increasing foliar capture and retention. Sprinkler irrigation emphasizes uniform water distribution and reasonable control of droplet kinetic input, aiming to alleviate surface runoff, soil crusting, and erosion risks.
- At the equipment scale, spray nozzles and irrigation sprinklers modulate application performance by adjusting internal flow structures, atomization characteristics, droplet size spectra, and spatial water distribution. Plant-protection nozzles aim to balance drift mitigation and canopy penetration performance, while advanced irrigation sprinklers attempt to alleviate inherent physical bottlenecks and coordinate low-pressure energy saving with spatial distribution uniformity.
- At the system scale, both fields are moving toward data-driven and energy-efficient operation. Variable-rate irrigation, precision spraying, UAV platforms, machine vision, and machine-learning-based prediction provide tools for improving resource-use efficiency, but their performance still depends on reliable coupling between fluid behavior, emitter design, and field conditions.
- Different from conventional single-domain review studies, this work establishes a generalized fluid dynamic framework to connect spray and irrigation equipment research. This review summarizes common design principles and cross-referable optimization strategies between the two fields, providing supplementary theoretical references for the future development of multifunctional spray and fertigation equipment.

6.2. Future Perspectives

Improving agricultural spray and sprinkler systems under variable weather, complex canopies, and heterogeneous soils requires further work in four directions:

- Drift, deposition, and soil-impact models should move beyond idealized wind-tunnel or laboratory conditions. Future studies should consider transient airflow, droplet breakup in turbulence, leaf vibration, and the effects of droplet ensembles on soil infiltration and runoff. Coupled CFD–multi-objective optimization frameworks will be critical to quantify cross-scale droplet transport and soil response.
- Intelligent real-time adaptive control and digital twin platforms represent a core emerging trend for integrated spraying systems. Low-cost multi-physical sensors will

feed real-time wind, temperature, humidity, canopy and soil data into digital twin models, which dynamically adjust operating pressure, flow rate, auxiliary airflow and working height via closed-loop feedback to match on-site variable field conditions.

- Data-driven modeling needs to overcome the limitations of pure black-box machine learning. While conventional algorithms have been used for spray performance prediction (Section 5.2), most lack embedded fluid physical constraints. Future work will prioritize physics-informed neural networks (PINNs). AI-assisted automatic nozzle structural optimization will be widely adopted to accelerate low-drift, low-impact emitter design.
- Eco-friendly, environmentally sustainable spray formulations remain an underexplored cross-disciplinary frontier. Next-generation rheological adjuvants and aerated liquid mixtures can tailor droplet size spectra simultaneously for plant-protection drift reduction and mild soil impact in fertigation integration, cutting chemical and water resource waste while mitigating off-target environmental pollution.
- Traditional pesticide sprayers and irrigation sprinklers are independently developed, leading to redundant field work and inconsistent droplet distribution. Future multifunctional intelligent platforms integrating pesticide spraying, fertigation and microclimate control can deliver evident synergy: shared liquid supply and control systems enable synchronous irrigation and chemical application in a single operation to boost efficiency and uniformity, which relies on interdisciplinary research covering agronomy, fluid mechanics, automation and data science.

Future development should focus on adaptive, energy-efficient, and data-supported agricultural fluid application systems rather than isolated improvements in individual nozzles or sprinklers.

Author Contributions: Conceptualization, S.-L.S. and W.Z.; methodology, J.-H.G.; software, K.D.; validation, S.-L.S., J.-H.G. and K.D.; formal analysis, W.Z.; investigation, W.Z.; resources, K.D.; data curation, J.-H.G.; writing—original draft preparation, S.-L.S. and K.D.; writing—review and editing, S.-L.S. and K.D.; visualization, S.-L.S.; supervision, J.-H.G.; project administration, W.Z.; funding acquisition, K.D. All authors have read and agreed to the published version of the manuscript.

Funding: This research was funded by Hangzhou International Innovation Institute, grant number 2025BKZ131.

Institutional Review Board Statement: Not applicable.

Informed Consent Statement: Not applicable.

Data Availability Statement: No new data were created or analyzed in this study.

Conflicts of Interest: Jian-Hui Gui was employed by Shimge (Zhejiang) Co., Ltd. The remaining authors declare that the research was conducted in the absence of any commercial or financial relationships that could be construed as a potential conflict of interest.

Abbreviations

AR	Application Rate
VMD	Volume Median Diameter
KEd	Droplet Kinetic Energy Per Unit Sprinkler Discharge
SP	Specific Power
KEa	Droplet Kinetic Energy Per Unit Area
PDA	Phase Doppler Anemometry
PIV	Particle Image Velocimetry
CFD	Computational Fluid Dynamics
S_{tk}	Stokes Number

DCAs	Drift Control Adjuvants
Eu_e	Electric Euler Number
We_e	Electric Weber Number
CMR	Charge-to-Mass Ratio
DV	Volume Median Diameter
Cd	Discharge Coefficient
CFS	Complete Fluidic Sprinkler
RSPS	Rotating Spray Plate Sprinkler
Eu	Euler Number
R^2	Coefficient of Determination
SD	Standard Deviation
CU/CUC	Christiansen's Uniformity Coefficient; Coefficient of Uniformity
DU	Distribution Uniformity
DPV	Drift Potential Value
CV	Coefficient of Variation
IS	Impact Sprinkler
AIS	Aeration Impact Sprinkler
DFS	Dynamic Fluidic Sprinkler
OS	Outside-Signal Fluidic Sprinkler
FSPS	Fixed Spray Plate Sprinkler
RS	Rotating Sprinkler
SFS	Spiral Fluidic Sprinkler
2DVD	2D Video Disdrometer
VFD	Variable Frequency Drive
LESA	Low Elevation Spray Application
ML	Machine Learning
MLR	Multiple Linear Regression
BP	Back Propagation (Neural Network)
RBF	Radial Basis Function Neural Network
RF	Random Forest
XGBoost/XGB	Extreme Gradient Boosting
RMSE	Root Mean Square Error
DD	Droplet Diameter
RSM	Response Surface Methodology
CUF	Coefficient of Uniformity for Fertigation
GA	Genetic Algorithm
NSGA-II	Nondominated Sorting Genetic Algorithm II
PINNs	Physics-Informed Neural Networks

References

1. Darko, R.O.; Yuan, S.Q.; Hong, L.; Liu, J.P.; Yan, H.F. Irrigation, a productive tool for food security—A review. *Acta Agric. Scand. Sect. B-Soil Plant Sci.* **2016**, *66*, 191–206.
2. Lakhiar, I.A.; Yan, H.F.; Syed, T.N.; Zhang, C.; Shaikh, S.A.; Rakibuzzaman, M.; Vistro, R.B. Agricultural Systems: Opportunities, Challenges, and Applications for Enhancing Horticultural Resilience to Climate Change and Urbanization. *Horticulturae* **2025**, *11*, 568. [CrossRef]
3. Faiçal, B.S.; Freitas, H.; Gomes, P.H.; Mano, L.Y.; Pessin, G.; de Carvalho, A.C.P.L.F.; Krishnamachari, B.; Ueyama, J. An adaptive approach for UAV-based pesticide spraying in dynamic environments. *Comput. Electron. Agric.* **2017**, *138*, 210–223. [CrossRef]
4. Gené-Mola, J.; Gregorio, E.; Guevara, J.; Auat, F.; Sanz-Cortiella, R.; Escolà, A.; Llorens, J.; Morros, J.-R.; Ruiz-Hidalgo, J.; Vilaplana, V.; et al. Fruit detection in an apple orchard using a mobile terrestrial laser scanner. *Biosyst. Eng.* **2019**, *187*, 171–184. [CrossRef]
5. Sarwar, A.; Peters, R.T.; Shafeeque, M.; Mohamed, A.; Arshad, A.; Ullah, I.; Saddique, N.; Muzammil, M.; Aslam, R.A. Accurate measurement of wind drift and evaporation losses could improve water application efficiency of sprinkler irrigation systems—A comparison of measuring techniques. *Agric. Water Manag.* **2021**, *258*, 107209. [CrossRef]

6. Chen, R.; Li, H.; Wang, J.; Song, Z.Y. Critical factors influencing soil runoff and erosion in sprinkler irrigation: Water application rate and droplet kinetic energy. *Agric. Water Manag.* **2023**, *283*, 108299. [CrossRef]
7. Jing, L.L.; Wei, X.H. Spray Deposition and Distribution on Rice as Affected by a Boom Sprayer with a Canopy-Opening Device. *Agriculture* **2023**, *13*, 94.
8. Chen, C.; Hussain, Z.; Liu, J.P.; Zaman, M.; Akhlaq, M. Innovative Technologies in Sprinkler Irrigation: An Overview. *Agriculture* **2024**, *58*, 799.
9. Hu, B.; Li, H.; Jiang, Y.; Tang, P.; Du, L. Review of the interaction mechanism for droplets and foliage under sprinkler irrigation and water-fertilizer integration. *Int. J. Agric. Biol. Eng.* **2024**, *17*, 31–43. [CrossRef]
10. Liu, J.P.; Liu, X.F.; Zhu, X.Y.; Yuan, S.Q. Droplet characterisation of a complete fluidic sprinkler with different nozzle dimensions. *Biosyst. Eng.* **2016**, *148*, 90–100. [CrossRef]
11. Xiang, Q.J.; Qureshi, W.A.; Tunio, M.H.; Solangi, K.A.; Xu, Z.D.; Lakhiar, I.A. low-pressure drop size distribution characterization of impact sprinkler jet nozzles with and without aeration. *Agric. Water Manag.* **2021**, *243*, 106458. [CrossRef]
12. Wang, G.; Li, Z.; Jia, W.; Ou, M.; Dong, X.; Zhang, Z. A Review on the Evolution of Air-Assisted Spraying in Orchards and the Associated Leaf Motion During Spraying. *Agriculture* **2025**, *15*, 964. [CrossRef]
13. Ma, J.; Liu, K.; Dong, X.Y.; Chen, C.G.; Qiu, B.J.; Zhang, S.C. Effects of Leaf Surface Roughness and Contact Angle on In Vivo Measurement of Droplet Retention. *Agronomy* **2022**, *12*, 2228. [CrossRef]
14. Jiang, Y.; Liu, J.; Li, H.; Hua, L.; Yong, Y. Droplet distribution characteristics of impact sprinklers with circular and noncircular nozzles: Effect of nozzle aspect ratios and equivalent diameters. *Biosyst. Eng.* **2021**, *212*, 200–214. [CrossRef]
15. Xu, T.; Li, X.; Lu, D.; Liu, Y.; Li, X.; Wang, S. Estimating the dynamic impact behavior of spray droplets on rice foliage. *Crop Prot.* **2025**, *197*, 107298. [CrossRef]
16. Šikalo, Š.; Ganić, E.N. Phenomena of droplet–surface interactions. *Exp. Therm. Fluid Sci.* **2006**, *31*, 97–110. [CrossRef]
17. Gong, C.; Jia, F.; Kang, C. Deposition of Water and Emulsion Hollow Droplets on Hydrophilic and Hydrophobic Surfaces. *Agriculture* **2024**, *14*, 960. [CrossRef]
18. Dong, X.; Dong, L.; Gao, Z.; Wang, K.; Wang, X.; Wang, S.; Qiu, B.; Wang, X. Droplet Deposition Behavior on the Surface of Flexible Pepper Leaves. *Agronomy* **2025**, *15*, 708. [CrossRef]
19. Cao, Y.; Wang, C.; An, Y.; Chen, Y.; Qiu, W. Droplet deposition behavior on the surface of wheat leaves with wind-induced vibration. *Crop Prot.* **2024**, *181*, 106699. [CrossRef]
20. Ahmad, F.; Zhang, S.; Qiu, B.; Ma, J.; Xin, H.; Qiu, W.; Ahmed, S.; Chandio, F.A.; Khaliq, A. Comparison of Water Sensitive Paper and Glass Strip Sampling Approaches to Access Spray Deposit by UAV Sprayers. *Agronomy* **2022**, *12*, 1302. [CrossRef]
21. Aksoy, Y.T.; Enayati, F.; Eneren, P.; Vetrano, M.R. Experimental study on enhanced heat transfer via nanoparticle depositions using TiO2-water nanofluid sprays. *Appl. Therm. Eng.* **2025**, *264*, 125450. [CrossRef]
22. Wu, M.M.; Dai, S.Q.; Ye, R.; Ou, M.X.; Wang, G.Q.; Hu, C.; Fan, X.R.; Jia, W.D. Experimental Study of Liquid Jet Atomization and Penetration in Subsonic Crossflows. *Agriculture* **2025**, *15*, 1037. [CrossRef]
23. Chen, R.; Li, H.; Wang, J.; Guo, X. Effects of Pressure and Nozzle Size on the Spray Characteristics of Low-Pressure Rotating Sprinklers. *Water* **2020**, *12*, 2904. [CrossRef]
24. Wang, J.; Song, Z.Y.; Chen, R.; Yang, T.; Tian, Z.K. Experimental Study on Droplet Characteristics of Rotating Sprinklers with Circular Nozzles and Diffuser. *Agriculture* **2022**, *12*, 987. [CrossRef]
25. Yue, J.; Chao, C.; Hong, L.; Xiang, Q.J. Influences of nozzle parameters and low-pressure on jet breakup and droplet characteristics. *Int. J. Agric. Biol. Eng.* **2016**, *9*, 22–32. [CrossRef]
26. Wang, Z.X.; Jiang, Y.; Liu, J.L.; Li, H.; Li, H. Experimental Study on Water Distribution and Droplet Kinetic Energy Intensity from Non-Circular Nozzles with Different Aspect Ratios. *Agriculture* **2022**, *12*, 2133. [CrossRef]
27. Liao, J.; Hewitt, A.J.; Wang, P.; Luo, X.W.; Zang, Y.; Zhou, Z.Y.; Lan, Y.B.; O'Donnell, C. Development of droplet characteristics prediction models for air induction nozzles based on wind tunnel tests. *Int. J. Agric. Biol. Eng.* **2019**, *12*, 1–6. [CrossRef]
28. Li, H.; Travlos, I.; Qi, L.; Kanatas, P.; Wang, P. Optimization of Herbicide Use: Study on Spreading and Evaporation Characteristics of Glyphosate-Organic Silicone Mixture Droplets on Weed Leaves. *Agronomy* **2019**, *9*, 547. [CrossRef]
29. Sedano, C.G.; Aguirre, C.A.; Brizuela, A.B. Numerical simulation of spray ejection from a nozzle for herbicide application: Comparison of drag coefficient expressions. *Comput. Electron. Agric.* **2019**, *157*, 136–145. [CrossRef]
30. Qin, C.; Loth, E. Numerical description of a pressure-swirl nozzle spray. *Chem. Eng. Process. Process Intensif.* **2016**, *107*, 68–79. [CrossRef]
31. Zhang, B.; Tang, Q.; Chen, L.-P.; Zhang, R.-R.; Xu, M. Numerical simulation of spray drift and deposition from a crop spraying aircraft using a CFD approach. *Biosyst. Eng.* **2018**, *166*, 184–199. [CrossRef]
32. Li, L.L.; Zhang, R.R.; Tang, Q.; Yan, W.L.; Ding, C.C.; Xu, G.; Yi, T.C. Predicting spray drift reduction classification of flat-fan nozzles based on droplet size spectrum. *Int. J. Agric. Biol. Eng.* **2025**, *18*, 24–32. [CrossRef]
33. Fattahi, S.H.; Pour, S.A. Sensitivity analysis of variables affecting spray drift from pesticides for their environmental risk assessments on agricultural lands. *Environ. Dev. Sustain.* **2025**, *27*, 13023–13043.

34. Ye, Q.; Shen, B.; Tiedje, O.; Domnick, J. Investigations of spray painting processes using an airless spray gun. In Proceedings of the 24th European Conference Liquid Atomization and Spray Systems, Estoril, Portugal, 5–7 September 2013.
35. Zhao, Y.; Huang, Y.; He, Z.; Zhong, W. Mini-review: Air-assisted spray nozzles and applications. *Front. Phys.* **2025**, *13*, 1705908. [CrossRef]
36. Gong, C.; Li, D.Y.; Kang, C. Visualization of the evolution of bubbles in the spray sheet discharged from the air-induction nozzle. *Pest. Manag. Sci.* **2022**, *78*, 1850–1860. [CrossRef] [PubMed]
37. Gong, C.; Li, D.Y.; Kang, C. Effect of oil-based emulsion on air bubbles in the spray sheet produced through the air-induction nozzle. *Pest. Manag. Sci.* **2022**, *78*, 5347–5357. [CrossRef] [PubMed]
38. Spanoghe, P.; De Schampheleire, M.; Van der Meeren, P.; Steurbaut, W. Influence of agricultural adjuvants on droplet spectra. *Pest. Manag. Sci.* **2007**, *63*, 4–16. [PubMed]
39. Lewis, R.W.; Evans, R.A.; Malic, N.; Saito, K.; Cameron, N.R. Polymeric drift control adjuvants for agricultural spraying. *Macromol. Chem. Phys.* **2016**, *217*, 2223–2242. [CrossRef]
40. Yan, M.; Chen, F.; Gong, C.; Kang, C. Characteristics of the Liquid Sheet of Air-Induction Spray. *Agronomy* **2025**, *15*, 1270. [CrossRef]
41. Wu, S.; Liu, J.Z.; Wang, J.S.; Hao, D.H.; Wang, R.K. The motion of strawberry leaves in an air-assisted spray field and its influence on droplet deposition. *Trans. ASABE* **2021**, *64*, 83–93. [CrossRef]
42. Zhou, Q.Q.; Xue, X.Y.; Chen, C.; Cai, C.; Jiao, Y.X. Canopy deposition characteristics of different orchard pesticide dose models. *Int. J. Agric. Biol. Eng.* **2023**, *16*, 1–6. [CrossRef]
43. Sánchez-Fernández, L.; Barrera, M.; Martínez-Guanter, J.; Pérez-Ruiz, M. Drift reduction in orchards through the use of an autonomous UAV system. *Comput. Electron. Agric.* **2023**, *211*, 107981. [CrossRef]
44. Sánchez-Fernández, L.; Alonso, E.; Ortiz-Barredo, A.; de Marti, S.P.; Jones, L.A.; Pérez-Ruiz, M. First UASS drift curves for agroforestry scenarios in Spain. *Crop Prot.* **2025**, *191*, 107164. [CrossRef]
45. He, Y.J.; Zhao, B.B.; Yu, Y.C. Effect, comparison and analysis of pesticide electrostatic spraying and traditional spraying. *Bulg. Chem. Commun.* **2016**, *48*, 340–344.
46. Dong, X.Y.; Wang, T.; Wang, S.F.; Ma, J.; Wang, K.Y.; Dong, L.L.; Qiu, B.J. Study on the Motion Behavior of Charged Droplets near Plant Leaves. *Horticulturae* **2025**, *11*, 1117. [CrossRef]
47. Zakaria, K.; Kamel, H.; Gamiel, Y. Instability of a viscous liquid sheet under the influence of a tangential electric field. *Alex. Eng. J.* **2022**, *61*, 5169–5181. [CrossRef]
48. Li, Y.F.; Li, Q.D.; Hu, J.; Liu, C.X.; Zhao, S.X.; Zhang, W.; Wang, Y.F. An Experimental Study on the Charging Effects and Atomization Characteristics of a Two-Stage Induction-Type Electrostatic Spraying System for Aerial Plant Protection. *Agronomy* **2025**, *15*, 1641. [CrossRef]
49. Gañán-Calvo, A.M.; Dávila, J.; Barrero, A. Current and droplet size in the electrospraying of liquids. Scaling laws. *J. Aerosol Sci.* **1997**, *28*, 249–275. [CrossRef]
50. Li, Y.F.; Zou, A.N.; Hu, J.; Liu, C.X.; Zhao, S.X.; Li, Q.D.; Zhang, W.; Wang, Y.F. Agricultural Electrostatic Spraying Electrode Corrosion Degradation Mechanisms: A Multi-Parameter Coupling Model. *Agriculture* **2025**, *15*, 1348. [CrossRef]
51. Duan, R.-Z.; Chen, Z.-Y.; Li, L. Linear stability analysis of an electrified viscoelastic liquid sheet ina viscous gas medium. *At. Sprays* **2014**, *24*, 155–179. [CrossRef]
52. Hu, H.M.; Kaizu, Y.; Huang, J.J.; Furuhashi, K.; Zhang, H.D.; Xiao, X.; Li, M.; Imou, K. Design and performance test of a novel UAV air-assisted electrostatic centrifugal spraying system. *Int. J. Agric. Biol. Eng.* **2022**, *15*, 34–40. [CrossRef]
53. Dai, S.Q.; Zhang, J.Y.; Jia, W.D.; Ou, M.X.; Zhou, H.T.; Dong, X.; Chen, H.; Wang, M.; Chen, Y.; Yang, S. Experimental Study on the Droplet Size and Charge-to-Mass Ratio of an Air-Assisted Electrostatic Nozzle. *Agriculture* **2022**, *12*, 889. [CrossRef]
54. Appah, S.; Wang, P.; Ou, M.X.; Gong, C.; Jia, W.D. Review of electrostatic system parameters, charged droplets characteristics and substrate impact behavior from pesticides spraying. *Int. J. Agric. Biol. Eng.* **2019**, *12*, 1–9. [CrossRef]
55. Dai, S.Q.; Wang, M.; Ou, M.X.; Zhou, H.T.; Jia, W.D.; Gao, R.H.; Wang, C.Y.; Wang, G.Q.; Li, Z.Y.; Chen, H. Development and Experiment of an Online Measuring System for Spray Deposition. *Agriculture* **2022**, *12*, 1195. [CrossRef]
56. Zhu, X.; Yuan, S.; Liu, J. Effect of sprinkler head geometrical parameters on hydraulic performance of fluidic sprinkler. *J. Irrig. Drain. Eng.* **2012**, *138*, 1019–1026. [CrossRef]
57. Liu, J.; Zhu, X.; Yuan, S.; Wan, J.; Chikangaise, P. Hydraulic Performance Assessment of Sprinkler Irrigation with Rotating Spray Plate Sprinklers in Indoor Experiments. *J. Irrig. Drain. Eng.* **2018**, *144*, 06018005. [CrossRef]
58. Zhou, X.; Li, Q.; Bi, J.; Cao, X.; Wang, Z.; Xu, X.; Zhang, Z.; Li, Y.; Jiang, X.; Chen, Y.; et al. Optimization of swirling-straight sprinklers in the pressurized spray systems of 200 MWt integrated nuclear heating reactors in China. *Nucl. Eng. Des.* **2025**, *435*, 113982. [CrossRef]
59. Qureshi, W.A.; Xiang, Q.; Tunio, M.H.; Qureshi, J.A.; Mosha, A.H.; Gao, J.; Elsherbiny, O. Optimization of inner flow dynamics in aeration impact sprinklers through CFD simulation, theoretical analysis, and experimental validation of stabilizer design for enhanced hydraulic performance. *Agric. Water Manag.* **2025**, *312*, 109463. [CrossRef]

60. Li, Y.F.; Liu, J.P.; Li, T.; Xu, J.E. Theoretical model and experiment on fluidic sprinkler wet radius under multi-factor. *J. Drain. Irrig. Mach. Eng.* **2018**, *36*, 685–689.
61. Zhou, X.; Li, H.; Pan, X.; Liu, J. Effects of rotational speed and working pressure on hydraulic performance of rotary sprinkler. *J. Drain. Irrig. Mach. Eng.* **2025**, *43*, 1291–1296.
62. Liu, J.P.; Zhu, X.Y.; Yuan, S.Q.; Liu, X.F. Droplet motion model and simulation of a complete fluidic sprinkler. *Trans. ASABE* **2018**, *61*, 1297–1306. [CrossRef]
63. Lakhiar, I.A.; Yan, H.F.; Zhang, C.; Wang, G.Q.; He, B.; Hao, B.B.; Han, Y.J.; Wang, B.Y.; Bao, R.X.; Syed, T.N.; et al. A Review of Precision Irrigation Water-Saving Technology under Changing Climate for Enhancing Water Use Efficiency, Crop Yield, and Environmental Footprints. *Agriculture* **2024**, *14*, 1141. [CrossRef]
64. Dwomoh, F.A.; Yuan, S.; Li, H.; Zhu, X.; Liu, J.; Mensah, R.; Fordjour, A. Analysis of Water Droplet Distribution in Wind for the Fluidic Sprinkler. *Water* **2020**, *12*, 3320. [CrossRef]
65. Darko, R.O.; Yuan, S.Q.; Liu, J.P.; Yan, H.F.; Zhu, X.Y. Overview of advances in improving uniformity and water use efficiency of sprinkler irrigation. *Int. J. Agric. Biol. Eng.* **2017**, *10*, 1–15.
66. Zhu, X.; Yuan, S.; Jiang, J.; Liu, J.; Liu, X. Comparison of fluidic and impact sprinklers based on hydraulic performance. *Irrig. Sci.* **2015**, *33*, 367–374. [CrossRef]
67. Li, P.; Wang, X.; Wu, W.; Yang, F.; Yuan, W. Research on the pulsed spraying characteristics of non-rotating deflector sprinklers. *Flow Meas. Instrum.* **2026**, *108*, 103202. [CrossRef]
68. Chen, R.; Chen, X.; Wang, J.; Guo, X.; Li, H. Regulation of soil nitrogen spatiotemporal variation by sprinkler irrigation patterns under surface fertilizer application. *Agric. Water Manag.* **2025**, *317*, 109654. [CrossRef]
69. Zhu, X.; Shi, Y.; Hu, G.; Liu, J. Dynamic Simulation and Test of Water Distribution of Fluidic Sprinkler. *J. Irrig. Drain.* **2020**, *39*, 74–83.
70. Fordjour, A.; Zhu, X.Y.; Jiang, C.L.; Liu, J.P. Effect of riser height on rotation uniformity and application rate of the dynamic fluidic sprinkler. *Irrig. Drain. Syst.* **2020**, *69*, 618–632. [CrossRef]
71. Lu, Y.Z.; Liu, P.F.; Montazar, A.; Paw, U.K.T.; Hu, Y.G. Soil Water Infiltration Model for Sprinkler Irrigation Control Strategy: A Case for Tea Plantation in Yangtze River Region. *Agriculture* **2019**, *9*, 206. [CrossRef]
72. Mohamed, A.Z.; Peters, R.T.; Zhu, X.Y.; Sarwar, A. Adjusting irrigation uniformity coefficients for unimportant variability on a small scale. *Agric. Water Manag.* **2019**, *213*, 1078–1083. [CrossRef]
73. Baiamonte, G.; Vaccaro, G. Normalised numerical analysis of uniformity coefficients for a newly referenced sprinkler area under square and equilateral triangle spacing arrangements. *Biosyst. Eng.* **2026**, *265*, 104343. [CrossRef]
74. Shi, Y.; Zhu, X.; Hu, G.; Zhang, A.; Li, J. Effect of different working conditions on water for sprinkler irrigation. *J. Drain. Irrig. Mach. Eng.* **2021**, *39*, 318–324. [CrossRef]
75. Chen, X.F.; Chen, R.; Wang, J.; Li, H.; Zhang, W.B. Evaluation of water distribution and uniformity of sprinkler irrigation based on harmonic analysis and finite element method. *Biosyst. Eng.* **2024**, *248*, 308–320. [CrossRef]
76. Yan, W.L.; Li, L.L.; Song, J.L.; Hu, P.; Xu, G.; Wu, Q.J.; Zhang, R.R.; Chen, L.P. Deep Learning-Assisted Measurement of Liquid Sheet Structure in the Atomization of Hydraulic Nozzle Spraying. *Agronomy* **2025**, *15*, 409. [CrossRef]
77. Hussain, Z.; Liu, J.P.; Chauhdary, J.N.; Zhao, Y.Y.; Wang, Y.B. Evaluating the hydraulic performance of rotating spray plate sprinklers. *J. Agric. Eng.* **2025**, *56*, 1773. [CrossRef]
78. Ahmed, S.; Qiu, B.J.; Ahmad, F.; Kong, C.W.; Xin, H. A State-of-the-Art Analysis of Obstacle Avoidance Methods from the Perspective of an Agricultural Sprayer UAV's Operation Scenario. *Agronomy* **2021**, *11*, 1069. [CrossRef]
79. Gong, C.; Li, D.Y.; Kang, C.; Wang, Y.L. Visualisation of the evolution of perforations in oil-based emulsion sheets formed by flat-fan spray nozzles. *Biosyst. Eng.* **2021**, *207*, 68–80. [CrossRef]
80. Tunio, M.H.; Gao, J.M.; Lakhiar, I.A.; Solangi, K.A.; Qureshi, W.A.; Shaikh, S.A.; Chen, J.D. Influence of Atomization Nozzles and Spraying Intervals on Growth, Biomass Yield, and Nutrient Uptake of Butter-Head Lettuce under Aeroponics System. *Agronomy* **2021**, *11*, 97. [CrossRef]
81. Wang, S.; Dorr, G.; Khashehchi, M.; He, X. Performance of selected agricultural spray nozzles using particle image velocimetry. *J. Agric. Sci. Technol.* **2015**, *17*, 601.
82. Gao, J.; Tunio, M.; Chen, Y.; He, R. Design and experiment of low-frequency ultrasonic nozzle integrating air-assistant system and acoustic levitation mechanism. *Int. J. Agric. Biol. Eng.* **2020**, *13*, 25–33. [CrossRef]
83. Gil, E.; Balsari, P.; Gallart, M.; Llorens, J.; Marucco, P.; Andersen, P.G.; Fàbregas, X.; Llop, J. Determination of drift potential of different flat fan nozzles on a boom sprayer using a test bench. *Crop Prot.* **2014**, *56*, 58–68. [CrossRef]
84. Yu, S.H.; Kang, Y.; Lee, C.G. Comparison of the Spray Effects of Air Induction Nozzles and Flat Fan Nozzles Installed on Agricultural Drones. *Appl. Sci.* **2023**, *13*, 11552. [CrossRef]
85. Guo, J.; Dong, X.; Qiu, B. Analysis of the Factors Affecting the Deposition Coverage of Air-Assisted Electrostatic Spray on Tomato Leaves. *Agronomy* **2024**, *14*, 1108. [CrossRef]

86. Farias, M.A.G.L.; Raetano, C.G.; Chechetto, R.G.; Ferreira-Filho, P.J.; Guerreiro, J.C.; Bonini, C.S.B.; Firmino, A.C.; Lima, R.C.; Prado, E.P. Spray nozzles and droplet size effects on soybean canopy deposits and stink bugs control in west region of São Paulo state—Brazil. *Phytoparasitica* **2020**, *48*, 203–213. [CrossRef]
87. Nuyttens, D.; Baetens, K.; De Schampheleire, M.; Sonck, B. Effect of nozzle type, size and pressure on spray droplet characteristics. *Biosyst. Eng.* **2007**, *97*, 333–345. [CrossRef]
88. Xu, S.; Jin, Y.; Zhong, Y.; Luo, L.; Song, J. Evaluation of spraying characteristics of a new multiple centrifugal nozzle applied to UAV. *Comput. Electron. Agric.* **2025**, *237*, 110712. [CrossRef]
89. Bayat, A.; Bozdogan, N.Y. An air-assisted spinning disc nozzle and its performance on spray deposition and reduction of drift potential. *Crop Prot.* **2005**, *24*, 951–960. [CrossRef]
90. Yao, W.; Chang, Y.; Liu, Y.; Xing, B.; Yan, H.; Sun, M.; Chen, C.; Lan, Y. Spray deposition characteristics of multi-rotor UAVs equipped with centrifugal nozzles on typical field crops. *Smart Agric. Technol.* **2025**, *12*, 101614. [CrossRef]
91. Gao, J.; Xu, K.; He, R.; Chen, X.; Tunio, M.H. Development and experiments of low frequency ultrasonic electrostatic atomizing nozzle with double resonators. *Int. J. Agric. Biol. Eng.* **2022**, *15*, 39–48. [CrossRef]
92. Knight, R.M.; Li, X.C.; Hocter, J.S.; Zhang, B.; Zhao, L.Y.; Zhu, H.P. Optimization of induction charging of water droplets to develop an electrostatic spray scrubber intended for poultry particulate matter mitigation. *J. ASABE* **2022**, *65*, 815–824. [CrossRef]
93. Lin, J.; Cai, J.; Ouyang, J.; Xiao, L.; Qiu, B. The Influence of Electrostatic Spraying with Waist-Shaped Charging Devices on the Distribution of Long-Range Air-Assisted Spray in Greenhouses. *Agronomy* **2024**, *14*, 2278. [CrossRef]
94. Ou, M.; Zhang, Y.; Zhang, T.; Wu, M.; Jia, W.; Dai, S.; Dong, X. Development and experiment of an air-assisted electrostatic nozzle and sprayer for vineyard pesticide application. *Crop Prot.* **2026**, *200*, 107455. [CrossRef]
95. Li, H.; Issaka, Z.; Jiang, Y.; Tang, P.; Chen, C. Overview of emerging technologies in sprinkler irrigation to optimize crop production. *Int. J. Agric. Biol. Eng.* **2019**, *12*, 1–9. [CrossRef]
96. Chauhdary, J.N.; Li, H.; Jiang, Y.; Pan, X.W.; Hussain, Z.; Javaid, M.; Rizwan, M. Advances in Sprinkler Irrigation: A Review in the Context of Precision Irrigation for Crop Production. *Agronomy* **2024**, *14*, 47. [CrossRef]
97. Xue, R.; Jiang, Y.; Li, H.; Shi, B. Review of advancements and challenges in delayed irrigation: Enhancing crop water productivity and sustainable crop production. *Agric. Water Manag.* **2025**, *318*, 109739. [CrossRef]
98. Jiang, Y.; Issaka, Z.; Li, H.; Tang, P.; Chen, C. Range formula based on angle of dispersion and nozzle configuration from an impact sprinkler. *Int. J. Agric. Biol. Eng.* **2019**, *12*, 97–105. [CrossRef]
99. Tang, P.; Li, H.; Issaka, Z.; Chen, C. Impact forces on the drive spoon of a large cannon irrigation sprinkler: Simple theory, CFD numerical simulation and validation. *Biosyst. Eng.* **2017**, *159*, 1–9. [CrossRef]
100. Issaka, Z.; Li, H.; Jiang, Y.; Tang, P.; Chen, C.; Fordjour, A. Comparative Evaluation On Performance Characteristics Of An Impact Sprinkler With Nozzle-Dispersion Devices And Rotary Plate Sprinkler. *Appl. Eng. Agric.* **2020**, *36*, 321–329. [CrossRef]
101. Pan, X.W.; Jiang, Y.; Li, H. Effects of the depth of the needle-shaped water dispersion device inserted into the jet on the jet breakup of sprinklers. *Irrig. Drain. Syst.* **2023**, *72*, 887–909. [CrossRef]
102. Li, H.; Issaka, Z.; Jiang, Y.; Tang, P.; Chen, C. Influence of a fixed water dispersion device on jet dispersion and range from an impact sprinkler. *Irrig. Drain.* **2019**, *68*, 669–678. [CrossRef]
103. Issaka, Z.; Li, H.; Jiang, Y.; Tang, P.; Chen, C.; Darko, R.O. Hydraulic performance characteristics of impact sprinkler with a fixed water dispersion device. *Int. J. Agric. Biol. Eng.* **2018**, *11*, 104–112. [CrossRef]
104. Coanda, H. Device for Deflecting a Stream of Elastic Fluid Projected into an Elastic Fluid. U.S. Patent 2,052,869, 1 September 1936.
105. Zhu, X.; Fordjour, A.; Yuan, S.; Dwomoh, F.; Ye, D. Evaluation of Hydraulic Performance Characteristics of a Newly Designed Dynamic Fluidic Sprinkler. *Water* **2018**, *10*, 1301. [CrossRef]
106. Hussain, L.; Khan, M.M.; Ahmad, N. Flow Performance Enhancement of a Fluidic Oscillator Through the Integration of Rectangular Ribs on Coanda Surface. *J. Fluids Eng.* **2024**, *146*, 111301. [CrossRef]
107. Fordjour, A.; Zhu, X.; Yuan, S.; Dwomoh, F.A.; Issaka, Z. Numerical simulation and experimental study on internal flow characteristic in the dynamic fluidic sprinkler. *Appl. Eng. Agric.* **2020**, *36*, 61–70. [CrossRef]
108. Zhu, X.; Fordjour, A.; Yuan, S.; Dwomoh, F.A.; Issaka, Z. Performance Optimization of A Newly Designed Dynamic Fluidic Sprinkler. *Appl. Eng. Agric.* **2021**, *37*, 33–41. [CrossRef]
109. Zhu, X.; Fordjour, A.; Dwomoh, F.A.; Lewballah, J.K.; Ofosu, S.A.; Liu, J.; Dai, X.; Oteng, J. Experimental study on the effects of pressure loss on uniformity, application rate and velocity on different working conditions using the dynamic fluidic sprinkler. *Heliyon* **2024**, *10*, e27140. [CrossRef] [PubMed]
110. Zhu, X.; Yuan, S.; Li, H.; Liu, J. Orthogonal tests and precipitation estimates for the outside signal fluidic sprinkler. *Irrig. Drain. Syst.* **2009**, *23*, 163–172. [CrossRef]
111. Jiang, Y.; Wang, Z.; Li, H.; Wang, L. Optimising the hydraulic performance of a jet impingement sprinkler by varying elevation angle: A Comparative study with a non-impingement sprinkler. *Biosyst. Eng.* **2024**, *245*, 24–35. [CrossRef]
112. Sourell, H.; Faci, J.M.; Playán, E. Performance of rotating spray plate sprinklers in indoor experiments. *J. Irrig. Drain. Eng.* **2003**, *129*, 376–380. [CrossRef]

113. Zhao, Y.Y.; Liu, J.P.; Hussain, Z. Multi-objective optimization of the fixed spray-plate sprinkler structure parameters of fertigation sprinkler based on response surface method. *Appl. Eng. Agric.* **2025**, *41*, 1–10. [CrossRef]
114. Issaka, Z.; Li, H.; Jiang, Y.; Tang, P.; Chao, C. Comparison of Rotation and Water Distribution Uniformity Using Dispersion Devices for Impact and Rotary Sprinklers. *Irrig. Drain.* **2019**, *68*, 881–892. [CrossRef]
115. Li, N.; Liu, J.; Zhou, N.; Yang, Q.; Liang, J.; Li, J.; Yu, L.; Liu, X.; Zhang, W. Characteristics of Rotary Sprinkler Water Distribution under Dynamic Water Pressure. *Horticulturae* **2022**, *8*, 804. [CrossRef]
116. Hua, L.; Li, H.; Bortolini, L.; Jiang, Y. A model for predicting effects of rotation variation on water distribution of rotary sprinkler. *Irrig. Sci.* **2023**, *42*, 677–688. [CrossRef]
117. Lewballah, J.K.; Zhu, X.; Fordjour, A.; Yao, S. Evaluation of Performance on Spiral Fluidic Sprinkler Using Different Nozzle Sizes Under Indoor Conditions. *Water* **2025**, *17*, 1745. [CrossRef]
118. Mughal, W.; Liu, J.; Ji, P.; Wang, W.; Luhur, M.R.; Abbasi, A.; Zhang, D. Performance Evaluation and Measurement Techniques for Agricultural Application Nozzles: A Systematic Review of Sprinkler and Pesticide Application Systems. *J. Appl. Fluid Mech.* **2026**, *19*, 588–619. [CrossRef]
119. Zhu, X.; Kong, J.; Fordjour, A.; Lewballah, J.K.; Dwomoh, F.A.; Ofosu, S.A.; Liu, J. Hydraulic performance assessment on dynamic fluidic and complete fluidic sprinklers under indoor and outdoor conditions. *J. Agric. Eng.* **2024**, *55*, 1580. [CrossRef]
120. Hussain, Z.; Liu, J.; Chauhdary, J.N.; Zhao, Y. Evaluating the effect of operating pressure, nozzle size and mounting height on droplet characteristics of rotating spray plate sprinkler. *Irrig. Sci.* **2025**, *43*, 1029–1044. [CrossRef]
121. Dwomoh, F.A.; Zhu, X.Y.; Fordjour, A.; Liu, J.P.; Yuan, S.Q.; Li, H. Structural design and performance characteristics of the fluidic sprinkler application technology for saving irrigation water: A review. *J. Agric. Eng.* **2023**, *54*, 1452. [CrossRef]
122. Liu, J.; Zhao, Y.; Pei, J.; Hussain, Z.; Mughal, W. Hydraulic Characterization of the External Flow Field of a Pressure-Self-Controlled Water-Pesticide Integrated Sprinkler. *J. ASABE* **2024**, *67*, 1133–1143. [CrossRef]
123. Chen, R.; Li, H.; Wang, J.; Guo, X.; Song, Z.Y. Comparisons of spray characteristics between non-circular and circular nozzles with rotating sprinklers. *Appl. Eng. Agric.* **2022**, *38*, 61–75. [CrossRef]
124. Mughal, W.; Pei, J.; Liu, J.; Wang, W.; Hussain, J.; Samo, I.A.; Rongjun, X.; Zhang, Y. Experimental investigation of flat fan nozzle V-cut depths and its impact on spray characteristics. *Sci. Rep.* **2025**, *15*, 22959. [CrossRef] [PubMed]
125. Hua, L.; Jiang, Y.; Li, H.; Qin, L. Effects of Different Nozzle Orifice Shapes on Water Droplet Characteristics for Sprinkler Irrigation. *Horticulturae* **2022**, *8*, 538. [CrossRef]
126. Wu, X.; Zhu, X.; Tan, M.; Liu, H.; Ge, J. Nozzle structure optimisation in a photovoltaic irrigation system. *Irrig. Drain.* **2024**, *74*, 900–914. [CrossRef]
127. Tarjuelo, J.M.; Rodriguez-Diaz, J.A.; Abadía, R.; Camacho, E.; Rocamora, C.; Moreno, M.A. Efficient water and energy use in irrigation modernization: Lessons from Spanish case studies. *Agric. Water Manag.* **2015**, *162*, 67–77. [CrossRef]
128. Yang, F.; Li, H.; Jiang, Y. A Review of Pressure Regulation Technologies for Irrigation Pipeline Systems. *Agriculture* **2025**, *15*, 1528. [CrossRef]
129. Chen, C.; Zhao, Y.; Liu, J.; Zhao, Y.; Hussain, Z.; Xie, R. Numerical Simulation of the Flow Field Stabilization of a Pressure-Regulating Device. *Agriculture* **2024**, *14*, 1873. [CrossRef]
130. Topak, R.; Suheri, S.; Ciftci, N.; Acar, B. Performance evaluation of sprinkler irrigation in a semi-arid area. *Pak. J. Biol. Sci.* **2005**, *8*, 97–103. [CrossRef]
131. Huang, X.; Dong, X.; Ma, J.; Liu, K.; Ahmed, S.; Lin, J.; Ahmad, F.; Qiu, B. Evaluation and Experiment of Flight Parameter Quality of the Plant Protection UAV Based on Laser Tracker. *Agriculture* **2021**, *11*, 628. [CrossRef]
132. Zhu, X.; Peters, T.; Neibling, H. Hydraulic Performance Assessment of Lesa at low Pressure. *Irrig. Drain.* **2016**, *65*, 530–536. [CrossRef]
133. Zhang, Q.; Ge, M.; Wu, P.; Wei, F.; Xue, S.; Wang, B.; Ge, X. Solar photovoltaic coupled with compressed air energy storage: A novel method for energy saving and high quality sprinkler irrigation. *Agric. Water Manag.* **2023**, *288*, 108496. [CrossRef]
134. Hui, X.; Lin, X.; Zhao, Y.; Xue, M.; Zhuo, Y.; Guo, H.; Xu, Y.; Yan, H. Assessing water distribution characteristics of a variable-rate irrigation system. *Agric. Water Manag.* **2022**, *260*, 107276. [CrossRef]
135. Zhang, L.Y.; Wang, A.C.; Zhang, H.Y.; Zhu, Q.Z.; Zhang, H.H.; Sun, W.H.; Niu, Y.X. Estimating Leaf Chlorophyll Content of Winter Wheat from UAV Multispectral Images Using Machine Learning Algorithms under Different Species, Growth Stages, and Nitrogen Stress Conditions. *Agriculture* **2024**, *14*, 1064. [CrossRef]
136. Zhao, J.M.Y.; Fan, S.X.; Zhang, B.H.; Wang, A.C.; Zhang, L.Y.; Zhu, Q.Z. Research Status and Development Trends of Deep Reinforcement Learning in the Intelligent Transformation of Agricultural Machinery. *Agriculture* **2025**, *15*, 1223. [CrossRef]
137. Jiang, L.; Xu, B.Y.; Husnain, N.; Wang, Q. Overview of Agricultural Machinery Automation Technology for Sustainable Agriculture. *Agriculture* **2025**, *15*, 1471. [CrossRef]
138. Du, Z.; Hu, Y.G.; Buttar, N.A. Analysis of mechanical properties for tea stem using grey relational analysis coupled with multiple linear regression. *Sci. Hortic.* **2020**, *260*, 108886. [CrossRef]

139. Skhiri, A.; Gabsi, K.; Dewidar, A.Z.; Mattar, M.A. Artificial Neural Networks versus Multiple Linear Regressions to Predict the Christiansen Uniformity Coefficient in Sprinkler Irrigation. *Agronomy* **2023**, *13*, 2979. [CrossRef]
140. Menezes, P.; Azevedo, C.; Eyng, E.; Neto, J.D.; Lima, V.L. Artificial neural network model for simulation of water distribution in sprinkle irrigation. *Rev. Bras. Eng. Agric. Ambient.* **2015**, *19*, 817–822. [CrossRef]
141. Hu, G.; Zhu, X.Y.; Yuan, S.Q.; Zhang, L.G.; Li, Y.F. Comparison of ranges of fluidic sprinkler predicted with BP and RBF neural network models. *J. Drain. Irrig. Mach. Eng.* **2019**, *37*, 263–269.
142. Elbeltagi, A.; Srivastava, A.; Deng, J.S.; Li, Z.B.; Raza, A.; Khadke, L.; Yu, Z.L.; El-Rawy, M. Forecasting vapor pressure deficit for agricultural water management using machine learning in semi-arid environments. *Agric. Water Manag.* **2023**, *283*, 108302. [CrossRef]
143. Yu, J.X.; Zhangzhong, L.; Lan, R.P.; Zhang, X.; Xu, L.L.; Li, J.J. Ensemble Learning Simulation Method for Hydraulic Characteristic Parameters of Emitters Driven by Limited Data. *Agriculture* **2023**, *13*, 986. [CrossRef]
144. Elhussiny, K.T.; Hassan, A.M.; Habssa, A.A.; Mokhtar, A. Prediction of water distribution uniformity of sprinkler irrigation system based on machine learning algorithms. *Sci. Rep.* **2023**, *13*, 20885. [CrossRef] [PubMed]
145. Hussain, Z.; Liu, J.; Chauhdary, J.N.; Md-Tahir, H.; Mokhtar, A. Predicting irrigation uniformity and droplet characteristics using machine learning algorithms for rotating spray plate sprinklers. *Flow Meas. Instrum.* **2026**, *110*, 103347. [CrossRef]
146. Shaikh, T.A.; Rasool, T.; Lone, F.R. Towards leveraging the role of machine learning and artificial intelligence in precision agriculture and smart farming. *Comput. Electron. Agric.* **2022**, *198*, 107119. [CrossRef]
147. Mowla, M.N.; Mowla, N.; Chowdhury, S.R.; Rabie, K.M.; Shongwe, T. Unmanned aerial vehicles (UAVs) for smart agriculture with machine learning: A system-oriented review of methods, applications, and challenges. *Smart Agric. Technol.* **2026**, *13*, 101880. [CrossRef]
148. Wang, P.; Hanif, A.S.; Yu, S.-H.; Lee, C.-G.; Kang, Y.H.; Lee, D.-H.; Han, X. Development of an autonomous drone spraying control system based on the coefficient of variation of spray distribution. *Comput. Electron. Agric.* **2024**, *227*, 109529. [CrossRef]
149. Zhang, C.; Xue, R.; Yan, H.F.; Lakhiar, I.A.; Ren, J.T.; Disasa, K.N.; Akhlaq, M.; Deng, S.S. Temperature-responsive regulation of combined drip and micro-sprinkler systems in greenhouses: An EWM-TOPSIS approach for enhancing tomato heat resilience and irrigation efficiency. *Irrig. Sci.* **2026**, *44*, 31. [CrossRef]
150. Wang, J.; Wei, T.; Song, Z.Y.; Chen, R.; He, Q. Determination of the Equivalent Length For Evaluating Local Head Losses In Drip Irrigation. *Appl. Eng. Agric.* **2022**, *38*, 49–59. [CrossRef]
151. Tang, P.; Zhang, Z.Z. Structural Optimization Based on Response Surface Methodology for the Venturi Injector Used in Fertigation System. *Horticulturae* **2025**, *11*, 223. [CrossRef]
152. Bonah, E.; Huang, X.Y.; Yang, H.Y.; Aheto, J.H.; Ren, Y.; Yu, S.S.; Tu, H.Y. Detection ofSalmonella Typhimuriumcontamination levels in fresh pork samples using electronic nose smellprints in tandem with support vector machine regression and metaheuristic optimization algorithms. *J. Food Sci. Technol.-Mysore* **2021**, *58*, 3861–3870. [CrossRef] [PubMed]
153. Kim, T. Optimization of fire sprinkler design for uniform water flux distribution using a micro-genetic algorithm. *Fire Saf. J.* **2024**, *144*, 104090. [CrossRef]
154. Pan, X.; Jiang, Y.; Li, H.; Bortolini, L. Design, optimization, and analysis of a new sprinkler with intermittent water-dispersing needle: Integration of RF-NSGA II algorithm and CFD simulation. *Comput. Electron. Agric.* **2024**, *222*, 109011. [CrossRef]
155. Li, H.; Pan, X.; Jiang, Y.; Zhou, X. Optimising and analysis of the hydraulic performance of a water dispersion needle sprinkler using RF-NSGA II and CFD. *Biosyst. Eng.* **2025**, *254*, 104113. [CrossRef]

Disclaimer/Publisher's Note: The statements, opinions and data contained in all publications are solely those of the individual author(s) and contributor(s) and not of MDPI and/or the editor(s). MDPI and/or the editor(s) disclaim responsibility for any injury to people or property resulting from any ideas, methods, instructions or products referred to in the content.